Evidence for influenza B virus hemagglutinin adaptation to the human host: high cleavability, acid-stability and preference for cool temperature

Running title: Adaptation of influenza B virus HA to human airways

Manon Laporte,[a] Annelies Stevaert,[a] Valerie Raeymaekers,[a] Talitha Boogaerts,[a] Inga Nehlmeier,[b] Winston Chiu,[a] Mohammed Benkheil,[a] Bart Vanaudenaerde,[c] Stefan Pöhlmann[b,d] and Lieve Naesens[a]#

[a]KU Leuven–University of Leuven, Department of Microbiology, Immunology and Transplantation, Rega Institute for Medical Research, Laboratory of Virology and Chemotherapy, Leuven, Belgium

[b]Infection Biology Unit, German Primate Center–Leibniz Institute for Primate Research, Göttingen, Germany

[c]KU Leuven–University of Leuven, Department of Chronic Diseases, Metabolism and Ageing, Laboratory of Pneumology, University Hospital Leuven, Leuven, Belgium

[d]Faculty of Biology and Psychology, University Göttingen, Göttingen, Germany

[#] Address correspondence to Lieve Naesens, lieve.naesens@kuleuven.be

Abstract

Influenza A virus (IAV) and influenza B virus (IBV) cause yearly epidemics with significant morbidity and mortality. When zoonotic IAVs enter the human population, the viral hemagglutinin (HA) requires adaptation to achieve sustained virus transmission. In contrast, IBV has been circulating in humans, its only host, for a long period of time. Whether this entailed adaptation of IBV HA to the human airways is unknown. To address this question, we compared seasonal IAV (A/H1N1 and A/H3N2) and IBV viruses (B/Victoria and B/Yamagata lineage) with regard to host-dependent activity of HA as the mediator of membrane fusion during viral entry. We first investigated proteolytic activation of HA, by covering all type II transmembrane serine protease (TTSP) and kallikrein enzymes, many of which proved present in human respiratory epithelium. Compared to IAV, the IBV HA0 precursor is cleaved by a broader panel of TTSPs and activated with much higher efficiency. Accordingly, knockdown of a single protease, TMPRSS2, was sufficient to abrogate spread of IAV but not IBV in human respiratory epithelial cells. Second, the HA fusion pH proved similar for IBV and human-adapted IAVs (one exception being HA of 1918 IAV). Third, IBV HA exhibited higher expression at 33°C, a temperature required for membrane fusion by B/Victoria HA. This indicates pronounced adaptation of IBV HA to the mildly acidic pH and cooler temperature of human upper airways. These distinct and intrinsic features of IBV HA are compatible with extensive host-adaptation during prolonged circulation of this respiratory virus in the human population.

Importance

Influenza epidemics are caused by influenza A (IAV) and influenza B (IBV) viruses. IBV causes substantial disease, however it is far less studied than IAV. While IAV originates from animal reservoirs, IBV circulates in humans only. Virus spread requires that the viral hemagglutinin (HA) is active and sufficiently stable in human airways. We here resolve how these mechanisms differ between IBV and IAV. Whereas human IAVs rely on one particular protease for HA activation, this is not the case for IBV. Superior activation of IBV by several proteases should enhance shedding of infectious particles. IBV HA exhibits acid-stability and a preference for 33°C, indicating pronounced adaptation to the human upper airways, where the pH is mildly acidic and a cooler temperature exists. These adaptive features are rationalized by the long existence of IBV in humans, and may have broader relevance for understanding the biology and evolution of respiratory viruses.

Introduction

The global burden of seasonal influenza is estimated at 3 to 5 million severe cases (1) and 290,000-650,000 fatalities per year (2). In addition, influenza A virus (IAV) causes sporadic pandemics with an even more severe impact on public health. Influenza B virus (IBV) does not cause pandemics but is responsible for a significant proportion of seasonal influenza (3). IBV may account for 22-44% of influenza deaths in children (3) and also elderly persons are at high risk (4). Between 1997 and 2009, IBV was the predominant cause of influenza-associated death in 4 out of 12 seasons (5). It was estimated that IAV and IBV diverged approximately 4,000 years ago (6). Current IBV strains fall into two lineages, B/Victoria and B/Yamagata, which diverged about 40 years ago and are now cocirculating globally (7). Gene reassortment between the two lineages is common yet not seen for the HA, PB1 and PB2 gene segments (7). Whereas IAV is widespread in birds and mammals (8), IBV is restricted to humans with no sustained animal reservoir (9) and only rare spillover events (10). When a zoonotic IAV enters the human population, adaptive changes in multiple viral proteins are required to achieve sustained human-to-human transmissibility (11). Which adaptive features were acquired by IBV as a result of its long existence in humans has hardly been investigated (9).

One major protein involved in this host adaptation is the viral hemagglutinin (HA), the mediator of viral entry (12, 13). HA binds to sialylated glycans on the cell surface to enable virus uptake by endocytosis. Next, HA mediates fusion of the viral envelope and endosomal membrane, allowing release of the viral genome into the cytoplasm. Membrane fusion occurs when virus-containing endosomes mature from early (pH ~6) to

late (pH ~5) endosomes, providing the low pH trigger for drastic refolding of HA and expulsion of its fusion peptide (14). To gain membrane fusion-competence, HA relies on host cell proteases for posttranslational cleavage of the HA0 precursor into two polypeptides, HA1 and HA2, a process termed priming or activation (15). In human IAV and IBV strains, HA0 has a monobasic (single arginine) cleavage site that is recognized by trypsin-like serine proteases. Understanding the protease dependency of HA might reveal biological differences between IAV and IBV, and direct drug concepts to target these proteases for influenza therapy (16, 17). A series of proteases have been proposed for IAV (reviewed by Böttcher-Friebertshäuser *et al*. (18)), but for IBV hardly any information is available. The type II transmembrane serine protease (TTSP) TMPRSS2 (transmembrane protease serine 2) is an activator of IAV HA0 in cell culture and essential for IAV replication in mice, at least for some IAV subtypes (19-22). In humans, a gene polymorphism leading to higher *TMPRSS2* expression was correlated with the risk for developing severe influenza (23). In cell culture, IAV can also be activated by some other TTSPs and kallikreins, but which of these support spread of IAV in human airways remains to be demonstrated [reviewed in: (16, 24)]. Regarding IBV, TMPRSS2 was shown to cleave IBV HA0 (17) and mediate virus spread in some human airway cell culture models (25), however this protease appeared dispensable for IBV pathogenesis in mice (26). Hence, the protease recognition profile of IBV HA is largely unknown.

Two other adaptive features of HA are related to its pH- and temperature-dependence. Again, data for IBV are very limited. Successful virus replication and transmission require a balance between the low pH that triggers HA refolding and membrane fusion during viral entry, and acid-stability of progeny virus in the respiratory tract and environment (27, 28).

Extracellular virions are sensitive to inactivation in mildly acidic parts of the upper respiratory tract (URT) like the nasal cavity (27, 29, 30). The acid-stability of HA appears to increase when a zoonotic IAV enters the human population and evolves into a human-to-human transmissible strain (31, 32). Studies in ferrets showed that increased IAV HA acid-stability contributes to airborne transmissibility (31, 33, 34). In addition, human airways exhibit a temperature gradient, from ~30-32°C in the nasal mucosa (35), to ~32°C in the upper trachea and ~36°C in the bronchi (36). Avian IAVs, adapted to the temperature of the avian enteric tract (40°C), show restricted growth at cooler temperatures (~32°C). Whereas the temperature dependency is fairly understood for the PB2 subunit of the viral polymerase (37), this is not the case for the viral surface glycoproteins, HA and neuraminidase (38). It is conceivable that HA proteins of IBV or human IAV might show intrinsic adaptation to the temperature of human airways, including the cooler temperature of the URT.

To understand how these human airway-specific factors may influence the membrane fusion activity of HA, we here compared the HA proteins of four seasonal human IAV and IBV viruses. Their proteolytic activation was analyzed by covering all members of the human TTSP (39) and kallikrein (KLK) families (40). We demonstrate that IBV HA exhibits much more efficient activation by a broad range of airway proteases, explaining why TMPRSS2 alone was required for spread of IAV but not IBV in human respiratory epithelial cells. Whereas the HA proteins of IBV and human IAV showed similar low pH-dependence to trigger membrane fusion, a distinction was seen in terms of temperature dependence, with IBV HA having clear preference for 33°C. For one of the two IBV lineages, this cooler temperature was required to achieve membrane fusion. We propose that these distinct

and intrinsic properties of the IBV HA protein might reflect extensive adaptation of IBV to the human respiratory tract.

Results

Human lung tissue and airway epithelial cell lines are rich in TTSP and KLK enzymes

Before investigating which TTSPs or KLKs are involved in HA activation of IAV or IBV, we assessed expression of these proteases in human airways. Their mRNA levels were quantified in tissue samples of healthy human lungs (from eight different donors; Figs 1A and 1B) and three continuous cell lines (Calu-3, 16HBE and A549) derived from human airways (Figs 1C and 1D). Lung tissue was shown to express abundant levels of *TMPRSS2* and *ST14/matriptase*. All other TTSPs showed high and comparable transcript levels, except for *TMPRSS11F* and *TMPRSS15* which were present at lower levels (Fig. 1A: left). These results agreed with microarray data for 108 healthy human lungs, retrieved from the GEO database (Fig. 1A: right). Human lung tissue contained high mRNA levels for several KLKs, but these showed more variable expression compared to the TTSPs (compare right panels of Figs 1A and 1B). Calu-3 and 16HBE cells (Figs 1C and 1D) showed abundant expression of *ST14/matriptase*, and Calu-3 cells also contained high levels of *TMPRSS2, TMPRSS3* and *TMPRSS4.* Both cell lines expressed several *KLK* transcripts. In A549 and HEK293T cells, expression of these proteases was generally lower. As expected, human lung tissue and the four cell lines abundantly expressed *FURIN*, which recognizes multibasic HA0 cleavage sites of highly pathogenic avian IAVs (41) (data not shown).

IBV HA0 is efficiently cleaved by a broad range of TTSPs

To investigate which of these proteases can activate the HA proteins of IAV or IBV, expression plasmids were generated for all 18 human TTSPs and 16 KLKs, bearing a C-terminal flag tag (for details see Table S1). When we analyzed expression in transfected cells, most proteases showed a protein level similar to that of TMPRSS2 regarded as the reference (Fig. S1C). For TMPRSS11B, TMPRSS12, TMPRSS7 and KLK13, expression was three-fold lower. For TMPRSS11D/HAT and TMPRSS11E/DESC1 expression was very weak, meaning that the results from the HA cleavage assay are an underestimate for these two proteases. In this assay, the proteases were co-expressed with the HAs from four seasonal IAV (A/H1 and A/H3) and IBV (B/Yam and B/Vic) viruses (Fig. 2A). HA0 cleavage was assessed by western blot for the HA1 or HA2 cleavage product, depending on which epitope was recognized by the anti-HA antibody. The % cleaved HA was calculated relative to the trypsin control, consisting of cells transfected with HA plus empty plasmid, and briefly exposed to exogenous trypsin.

TMPRSS2 was the only protease that efficiently cleaved all four IAV/IBV HA0 proteins tested. It was the only protease with high activity on A/H3 HA0 (Fig. 2B and 2C), while A/H1 HA0 was equally well cleaved by TMPRSS4. On the other hand, the two IBV HA0 proteins were efficiently processed by four TTSPs (Fig. 2B and 2C), namely TMPRSS11F, TMPRSS2, TMPRSS4, and TMPRSS13/MSPL. Besides, IBV HA0 was cleaved by TMPRSS11A and TMPRSS11D/HAT, yet low expression of the latter protease (see above) precluded conclusions on cleavage efficiency. B/Yam HA0 was also recognized by TMPRSS5 and TMPRSS6. One TTSP, namely Hepsin, generated weak bands for both HA0 and HA1/HA2 (Fig. 2B), indicating HA degradation as observed before (42). Finally,

none of the kallikreins was found to be a broad HA activator. KLK14 cleaved both IBV proteins, and KLK5 and KLK6 cleaved B/Yam HA0 with low efficacy. In summary, we demonstrated that, compared to its IAV counterpart, IBV HA0 can use a broader panel of TTSPs for efficient proteolytic cleavage.

All HA0-cleaving TTSPs generate membrane fusion-competent IBV HA

We next examined whether HA0 cleavage translates into HA activation. We first employed a polykaryon assay (Fig. 3A) in which HeLa cells that co-express HA and protease, are exposed to acidic pH to trigger HA-mediated cell-cell fusion. IBV HA generated abundant polykaryons (Fig. 3B) when co-expressed with TMPRSS11F, TMPRSS2, TMPRSS4, and TMPRSS13/MSPL, consistent with efficient cleavage by these four TTSPs in the western blot assay (see above). A lower number of polykaryons was seen for TMPRSS11D/HAT, TMPRSS11A, Hepsin, TMPRSS5 and TMPRSS6. All these TTSPs thus generate a fusion-competent HA1-HA2 protein, meaning that they cleave IBV HA0 at the correct position. No polykaryons were formed in cells expressing KLK5, KLK6 or KLK14 (Fig. 3B). For KLK5 and KLK6, the levels of cleaved HA (Fig. 2) were probably too low to induce membrane fusion. KLK14 likely cleaves the IBV HA0 protein at an incorrect position, since the HA2 product generated by KLK14 migrated slightly slower (Fig. 2B) than that produced by trypsin or an activating TTSP.

IBV shows superior TTSP activation for viral entry

To verify that the TTSPs activate HA for membrane fusion during viral entry, we employed a retroviral pseudotyping system (Fig. 4A). Each HA was combined with its cognate neuraminidase (NA) to assure efficient particle release (43, 44). Pseudoparticles were

197 produced in the presence or absence of TTSPs, treated with PBS or trypsin and then
198 examined for their ability to transduce target cells (Fig. 4A). In Fig. 4B and 4C, the colored
199 bars show transduction efficiency of TTSP-activated particles, whereas the white bars
200 show total particle infectivity upon additional treatment with trypsin.
201 For the two seasonal IAVs, pseudoparticles produced in the presence of TMPRSS2 and
202 TMPRSS11D/HAT (now generated from a pCAGGS-based plasmid to bypass low
203 expression; see above) transduced cells with the same efficiency as trypsin-treated
204 control particles (indicated with the dashed line in Figs 4B and 4C). Particles carrying A/H1
205 HA, but not A/H3 HA, were also fully activated by TMPRSS4. Accordingly, transduction
206 efficiency by these particles was only slightly increased when they were treated with
207 trypsin. In sharp contrast, IBV pseudotypes produced in the presence of Hepsin,
208 TMPRSS2, TMPRSS4, TMPRSS13/MSPL, TMPRSS11D/HAT and TMPRSS11E/DESC1
209 (for B/Yam), transduced cells with markedly higher efficiency than control particles
210 activated by trypsin (Fig. 4B). For instance, B/Yam particles activated by TMPRSS2 or
211 TMPRSS11D/HAT generated approximately 2000-fold higher signals than the trypsin
212 control. This superior activation of the IBV particles was also evident from the observation
213 that subsequent trypsin treatment gave a lower signal increase for the IBV compared to
214 the IAV particles (see white bars in Fig. 4B).
215
216 To investigate the possibility that the efficiency of HA activation might be linked to IAV
217 virulence or pandemic potential, we included pseudotypes derived from 1918 A/H1N1 IAV
218 and avian A/H7N9 IAV, which both possess a monobasic HA0 cleavage site. The former
219 virus caused the devastating 1918 pandemic, and its HA protein was identified as a
220 virulence determinant (45, 46) although the underlying mechanism is not understood (47,

48). A high case-fatality rate in humans is also seen with avian A/H7N9 IAV, which is feared for its pandemic potential (49). The three A/H1N1 pseudotypes tested, i.e. derived from 1918 IAV, 2009 pandemic virus and the laboratory strain A/PR/8/34 (PR8), as well as the A/H7N9 subtype, shared TMPRSS2 and TMPRSS4 as the most effective HA-activators (Fig. 4C). Hence, whereas TTSP activation was clearly more efficient for IBV compared to IAV pseudotypes, such a difference was not seen for highly virulent *versus* seasonal IAVs. On the other hand, 1918 IAV-pseudoparticles showed 10- and 100-fold higher transduction efficiency than the PR8- and Virg09-pseudotypes, respectively (Fig. S2) Since the three A/H1N1 pseudotypes showed comparable incorporation of HA and MLV gag and a similar level of HA0 cleavage (Fig. S2), the difference might be related to the HA fusion pH (see below) (28). An alternative explanation may be that the 1918 IAV neuraminidase, present on these pseudoparticles, may have enhanced their entry process (50).

To summarize, these polykaryon and pseudoparticle experiments established ten TTSPs as moderate to strong HA activators. Compared to the IAV proteins, IBV HA exhibits superior activation by a broader range of TTSPs.

IBV but not IAV employs several proteases for spread in human airway-derived Calu-3 cells

Since Calu-3 cells show a similar TTSP and KLK expression profile as healthy human lungs (see above), they are a good model to study the role of these proteases in virus activation in the human respiratory tract. For the four IAV/IBV strains, i.e. Virg09 (A/H1N1), HK68 (A/H3N2), Ned05 (B/Yam) and Mal04 (B/Vic), multicycle (i.e. zanamivir-sensitive,

Table S5) replication in Calu-3 cells was the same whether trypsin was added or not (*P*-value > 0.1, Fig. S3), meaning that these cells express one or more HA0-activating proteases. The four viruses were similarly inhibited by three serine protease inhibitors (see antiviral EC_{50} values in Table S5; a brief description of the assay is provided below this Table) but were not blocked by a furin inhibitor, consistent with furin's inability to process monobasic HA0 cleavage sites (41). We also observed no effect with inhibitors of lysosomal cathepsins, which activate some unrelated viruses that enter by endocytosis (51). Thus, HA activation in Calu-3 cells relies on one or more serine proteases.

After optimizing the procedure for robust siRNA-mediated gene knockdown in Calu-3 cells (Fig. S4), we performed broad knockdown for the 18 TTSPs and 16 KLKs. To assess the impact of protease knockdown on IAV or IBV replication, virus was added 48 h after siRNA transfection, and virus infection was monitored at day 3 p.i. by high-content imaging of NP immunostaining (Fig. 5A). None of the siRNAs produced unwanted cytotoxic effects, the only exception being TMPRSS6 knockdown which reduced cell viability by 40% (Fig. 5B). TMPRSS2 was the only protease for which knockdown caused significant (*P*-value = 0.0001) reduction in replication of A/H1N1 and A/H3N2 virus (Fig. 5B and 5C). In sharp contrast, IBV infection was only marginally (Fig. 5B, B/Yam: *P*-value = 0.047) or not (Fig. 5B, B/Vic: *P*-value = 0.48) reduced by TMPRSS2 knockdown. Finally, IBV was not affected by single knockdown of any TTSP or KLK, nor by combined knockdown of TMPRSS2 and the most efficacious IBV HA activators identified above (Fig. 5D). Hence, the spread of IBV appears to rely on redundant proteases, concurring with the above findings that, besides TMPRSS2, several proteases effectively activate the IBV HA protein.

TMPRSS4 is abundant in MDCK cells yet dispensable for spread of IBV in these cells

To assess whether some TTSPs might stand out as activators of IBV, we included Madin-Darby canine kidney (MDCK) cells which, alike Calu-3 cells, support replication of IBV in the absence of trypsin (52). This observation was also made for 1918 IAV (50, 53) which, in this regard, is unique among human IAV strains. Indeed, our seasonal IBV but not IAV viruses did not require exogenous trypsin to replicate in MDCK cells (Fig. 6A). HA0 cleavage during IBV replication was inhibited by the broad serine protease inhibitor camostat (Fig. 6B), hence executed by one or more proteases of this family. mRNA quantification in MDCK cells (see Table S3 for dog-specific primers) revealed abundant expression of *ST14/matriptase*, as observed before (54, 55) and *TMPRSS4* (Fig. 6C). Another study (50) found no *TMPRSS4* mRNA in MDCK cells, potentially related to the use of different MDCK cell lines (56). Canine TMPRSS4 was cloned into an expression plasmid to investigate its HA0-cleaving capacity. Canine TMPRSS4 proved a strong activator for IBV HA, and more effective on A/H1 HA from 1918 IAV compared to 2009 pandemic (Virg09) IAV (Fig. 6D). The lowest efficiency was seen for A/H3 HA. The polykaryon assay confirmed that fusion-competent HA was formed (pictures in Fig. 6D).

The mRNA data suggested that canine TMPRSS4 or ST14/matriptase might be responsible for spread of IBV in MDCK cells. For IAV HA, published data on the role of matriptase are not consistent (55, 57, 58). Although our data thus far argued against a direct role for matriptase, an indirect role (e.g. as an activator of TMPRSS4) could not be excluded. With this is mind, we performed knockdown for canine TMPRSS4 and matriptase individually or in combination (Fig. 6E and 6F). Knockdown efficiency was >85% based on RT-qPCR for mRNA. Virus replication and HA0 cleavage in IBV-infected

MDCK cells proved unaffected by knockdown of TMPRSS4, matriptase, nor a combination of the two (Fig. 6F). Thus, both in Calu-3 and MDCK cells, IBV does not seem to rely on one single protease for its replication.

IBV HA exhibits a similar fusion pH as human-adapted IAV HAs

Cleavage of HA0 into HA1-HA2 activates the protein for membrane fusion, but also renders HA susceptible to inactivation at acidic pH. The human nasal cavity is mildly acidic (average pH: 6.3 in healthy adults and 5.9 in children) (30, 59). For pandemic IAV, acquirement of a more acid-stable HA is considered a prerequisite to achieve human-to-human transmissibility (27, 31, 43, 60). Since IBV is restricted to humans, we asked whether IBV possesses an acid-stable HA. Indeed, the polykaryon assay showed that the two IBV HA (i.e. B/Yam and B/Vic) proteins have a fusion pH value in the same range (5.4-5.6) as their human IAV counterparts (Fig. 7B-D), while avian A/H5 and A/H7 HAs had higher values (5.7 and 5.8, respectively; Fig. 7E), in line with previous reports (34, 43, 61, 62). On the other hand, the shape of the pH curves was distinct for IBV HA. For human-adapted IAV HAs, the curves showed a discrete pH value at which the number of polykaryons was maximal, and a steep decline at more acidic pH due to HA inactivation (63). In contrast, both IBV HAs produced high numbers of polykaryons over the entire low pH range. Hence, IBV HA is triggered for fusion at a similar acidic pH as IAV HA, however the IBV protein may be more resistant to acidic conditions. Besides, we noticed that 1918 A/H1 HA (Fig. 7D) had the highest fusion pH among the tested human IAV HAs, its value (5.7) being as high as that of avian A/H5 HA (Fig. 7E). This might explain the superior transduction efficiency of 1918 IAV pseudoparticles (see above), since an increased fusion pH enables earlier endosomal escape and more efficient infection (28).

A temperature of 33°C is preferred by IBV HA and required for fusion by the B/Victoria lineage

The human URT has a temperature (~30-32°C) below body temperature (35, 36) and well below that of the avian intestinal tract (~40°C) (64, 65). Since a temperature of 33°C is preferred for propagating IBV in cell culture, we investigated whether HA has an intrinsic role in this temperature preference. Protein expression of IBV HA proved to be temperature-dependent, being highest at 33°C and gradually decreasing at higher temperatures (Fig. 8A). The 33°C preference was seen for both IBV lineages but was particularly significant for B/Vic HA (*P*-value = 0.0006 for comparison of protein levels at 33°C and 37°C). For human IAV and avian A/H5 HAs, expression was similar within the range of 33-39°C, although for A/H1 HAs, it tended to be highest at 39°C. Avian A/H7 HA manifested a clear preference for 39°C (Fig. 8A).

When the polykaryon assay was conducted at 37°C, B/Vic HA proved unable to induce membrane fusion at any pH tested (Fig. 8D), however abundant polykaryons were formed at 33°C (Fig. 8B and 8C). Varying the temperature during protein expression or membrane fusion (see arrow schemes in Fig. 8B) revealed that the 33°C requirement was due to inefficient HA expression at 37°C. Whether cell-cell fusion took place at 33°C or 37°C made no difference. Due to low expression at 37°C, the levels of activated HA, generated by trypsin, were undetectable (Fig. 8D). The strict 33°C requirement was not seen with B/Yam HA, since this protein generated polykaryons at all temperatures, including at 39°C (Fig. 8B). The HA of the B/Vic lineage carries a globular head glycan at residue N248, that is lacking in the B/Yam lineage (7, 66, 67). When we substituted N248 in B/Vic HA by D248, the corresponding residue in B/Yam HA, the pH threshold to induce polykaryons shifted from 5.4 to 5.5 (Fig. 8C). Polykaryons induced by the N248D-mutant were larger

and more numerous compared to wild-type B/Vic HA (Fig. 8B and 8C). However, the mutation did not change the 33°C preference for protein expression and membrane fusion (Fig. 8B-D), indicating that this N248 glycan is not responsible for the temperature-sensitive phenotype of B/Vic HA.

Accordingly, pseudoparticles carrying B/Vic HA produced at 33°C had much higher infectivity compared to those generated at 37°C (*P*-value < 0.0001, Fig. 9B). Transduction efficiency was similar at both temperatures. At the cooler temperature, higher HA protein levels were visible in the producer cells and particularly in released pseudoparticles (Fig. 9C), suggesting that this reduced temperature may be required for efficient posttranslational transport and membrane incorporation of B/Vic HA.

In combination, these results indicate a possible correlation between HA expression and host temperature, with IBV HA preferring 33°C, the temperature of the human URT, and avian A/H7 HA preferring the body temperature of birds. The 33°C preference was stricter for B/Vic HA than for B/Yam HA, a difference unrelated to the lineage-specific N248 head glycan.

Discussion

Compared to the large body of literature on the HA proteins from human and zoonotic IAVs and how some of their properties reflect viral host-adaptation (8, 27), the HA of IBV is far less characterized (9). In this study, we compared the HA proteins of human IAV and IBV in terms of proteolytic activation, pH stability and temperature preference, as markers for host adaptation. Our results provide evidence for more pronounced adaptation of IBV HA to the human airways, in keeping with the long and exclusive circulation of IBV in humans.

In order to be membrane fusion-competent, HA requires cleavage by a host cell protease. Several TTSPs and KLKs have been linked to IAV HA activation (reviewed in (18)), yet a comprehensive analysis was, thus far, missing for IAV and especially for IBV. To close this gap, we compared all 18 human TTSP and 16 KLK enzymes for their capacity to cleave and activate the IAV and IBV HA proteins. Our results confirm the leading role of TMPRSS2 in activation of monobasic IAV HAs, consistent with data obtained in cell culture, knockout mice or humans (19, 20, 23). The report that TMPRSS2 proved dispensable for spread of IBV in mice (26) suggested that either TMPRSS2 is not involved at all or several redundant proteases may activate IBV HA. Our findings support the latter assumption, since the cleavability of IBV HA proved clearly superior to that of IAV. We demonstrated that both IBV HA lineages are cleaved and activated by a broad range of (in total ten) TTSP enzymes, the strongest activators being TMPRSS2, TMPRSS4, TMPRSS11F, TMPRSS13/MSPL, Hepsin and TMPRSS11D/HAT, followed by four other proteases (TMPRSS5, TMPRSS6, TMPRSS11A and TMPRSS11E/DESC1). All these

TTSPs are expressed in human lung tissue and generate a functional, i.e. membrane fusion-competent, IBV HA protein. In contrast, activation of A/H1N1 and A/H3N2 HA was largely limited to TMPRSS2 and TMPRSS11D/HAT, and TMPRSS4 in the case of A/H1N1. We saw no evidence for a role of TMPRSS15/enterokinase (Hayashi 2018) or KLK5, KLK12 (68, 69) or any other kallikrein. It is possible that the KLK levels attained in our cell systems were below those applied during incubation with recombinant KLKs (68). Finally, our data do not support involvement of ST14/matriptase in cleavage of A/H1 HA (57, 58), in line with another report (55).

Limburg et al. recently showed that TMPRSS2 was crucial for IBV activation in human primary type II alveolar epithelial cells, but dispensable for spread in primary human bronchial epithelial cells and Calu-3 cells, pointing to as yet unspecified protease(s) (25). We show that single knockdown of none of the 18 TTSPs had an impact on IBV replication in Calu-3 cells, and also dual knockdown of TMPRSS2 plus another HA-activating TTSP had no effect, supporting the hypothesis that IBV can rely on redundant proteases for HA activation. This is also evident from our observation in MDCK cells, in which knockdown of the abundantly expressed TMPRSS4 nor matriptase could halt IBV replication. In contrast, replication of A/H1N1 and A/H3N2 viruses in Calu-3 cells proved strongly dependent on TMPRSS2. This is noteworthy considering that TMPRSS4 efficiently activated A/H1 HA in transfected cells and proved abundantly expressed in Calu-3 cells. How can this central role of TMPRSS2 in activation of IAV HA be explained? Unlike other TTSPs, TMPRSS2 may be present at high levels in all compartments of the constitutive secretory pathway (70) which is also followed by HA. Only TMPRSS2 appears to extensively colocalize with HA (71). Also, TMPRSS2 might not only activate HA but also

the viral M2 ion channel (72). Why is IBV HA more efficiently activated than IAV HA? It is plausible that IBV HA may exhibit higher TTSP accessibility, perhaps governed by the dynamics of HA glycoprotein folding, maturation, or transport towards the cell membrane. This might be influenced by *N*-glycans in the HA head or stem (at sites very distant from the cleavage loop) having an effect on HA folding rate (73). An *N*-glycan (N8) located at the bottom of the A/H3 HA stem was shown to retard HA folding (73) and be lost when an A/H3N2 virus was passaged in TMPRSS2-knockout mice (74). Another factor is the HA0 cleavage site itself, for which two differences between IBV and IAV may be relevant: (i) at position P3 (P1 being the scissile arginine), IBV HA0 contains an extra basic lysine residue while A/H1 and A/H3 HAs carry a glutamine; and (ii) the P2' residue is phenylalanine in IBV but leucine, a less hydrophobic residue, in human IAV HAs. Besides, the IBV HA0 cleavage loop might be structurally distinct from the A/H1 and A/H3 HA0 loops. While the latter two have been resolved (75, 76), an X-ray structure of IBV HA0 is still missing.

Since the clinical picture of IBV is similar to that of IAV (9), the high cleavability of IBV HA appears not linked to virulence. However, it assures shedding of infectious virus. Human-to-human transmissibility also requires optimal HA acid-stability, since this renders the virus more stable under mildly acidic conditions in the human URT or environment (27). For zoonotic IAVs, adaptation to the human host is associated with HA stabilization, reducing the HA fusion pH to 5.2-5.5 (31). This fits with the fusion pH values that we measured for IBV HA, i.e. 5.4 for the B/Victoria and 5.6 for the B/Yamagata lineage. Literature data for IBV are scarce but our values are in agreement with other reports (77, 78). The difference in fusion pH between the two lineages appears partially related to the B/Victoria lineage-specific N248 HA head glycan, positioned adjacent to the receptor

binding site (7). Removing this *N*-glycan caused a small increase in the fusion pH threshold, pointing to an allosteric effect of the HA head domain on the fusion process, which is consistent with a role for receptor binding in fusion peptide dynamics (14).

For both IBV lineages, HA exhibits an intrinsic preference for 33°C which is particularly pronounced for the B/Victoria lineage. Analysis of additional IBV strains could validate our hypothesis that, compared to the B/Yamagata lineage, B/Victoria HA might be even better adapted to the proximal airways, given its stricter 33°C dependence and lower fusion pH. Its more stable HA could perhaps explain higher prevalence of this lineage in children (9) which typically have a more acidic nasal pH (27). A preference for cooler temperature was also reported for the hemagglutinin-esterase-fusion (HEF) protein of influenza C virus, which mainly infects humans (79). We did not observe this temperature effect for human IAV HAs, and saw the opposite pattern for avian A/H7 HA. This leads us to hypothesize that fine-tuning of HA protein expression to fit the temperature of the host target organs could be another viral adaptation strategy, besides well-known mechanisms related to receptor use, polymerase activity or immune evasion (8). The temperature-sensitive expression of IBV HA is an intrinsic feature seen in the absence of any other IBV proteins, hence it is unrelated to the reduced RNA synthesis seen with some temperature-sensitive IBV strains (80). As for the biochemical basis, for influenza C virus HEF, trimer formation and surface expression proved more efficient at 33°C than at 37°C (79). A similar temperature effect probably applies to IBV HA, since pseudoparticles carrying B/Vic HA contained much higher HA levels when produced at 33°C compared to 37°C. For IAV HA, a link exists between *N*-glycosylation and temperature sensitivity of the processes of HA folding or transport towards the cell membrane (73, 81-84). We therefore examined the

role of the B/Victoria lineage-specific N248 glycan, however, removal of this HA head *N*-glycan did not change the dependence on 33°C.

Although our study was focused on the HA proteins of seasonal human IAV and IBV viruses, we also made an interesting observation for the HA of 1918 IAV. Its HA fusion pH (5.7) proved to be exceptionally high for a human IAV but identical to that of highly pathogenic avian A/H5N1 virus. This may help to explain the exceptional virulence of 1918 IAV, since IAVs with high HA fusion pH evade interferon control (85) and are more virulent in mice (86). It could also rationalize a mouse study in which the 1918 HA protein by itself generated a highly pathogenic phenotype when introduced in a contemporary backbone virus (46). Besides, we showed that TTSP activation is comparable for 1918 HA and other A/H1 HAs. Hence, the unique capacity of 1918 IAV to replicate in MDCK cells in the absence of trypsin (50, 53) seems not, or at least not entirely, explained by HA activation by TMPRSS4 or another TTSP expressed in MDCK cells. As proposed (53, 87), a role for the 1918 IAV neuraminidase is plausible.

To conclude, we demonstrated that the IBV HA protein combines broad and efficient activation capacity, favorable acid-stability and preference for the cooler temperature of the human URT. These distinct properties likely reflect host-adaptation resulting from sustained presence of this respiratory pathogen in the human population.

Materials and methods

Ethics statement

Lung tissue samples from eight different healthy donors were obtained under the approval of the ethical committee from the University Hospital Leuven (UZ Leuven Biobanking S51577). All patients were adult and provided written informed consent.

Cells, media and compounds

Calu-3 (ATCC #HTB-55), A549 (ATCC #CCL-185), 16HBE [a gift from P. Hoet (Leuven, Belgium)] and HeLa (ATCC #CCL-2) cells were grown in Minimum Essential Medium (MEM) supplemented with 10% fetal calf serum (FCS), 0.1 mM non-essential amino acids, 2 mM L-glutamine and 10 mM HEPES. HEK293T cells (Thermo Fisher Scientific #HCL4517) and Madin-Darby canine kidney (MDCK) cells, a gift from M. Matrosovich (Marburg, Germany), were grown in Dulbecco's modified Eagle's Medium supplemented with 10% FCS, 1 mM sodium pyruvate and 0.075% sodium bicarbonate. Medium with reduced (i.e. 0.2%) FCS content was used during protease expression and virus infection experiments. Except stated otherwise, all cell incubations were done at 37°C. The following compounds were purchased from Sigma-Aldrich: N-tosyl-L-phenylalanine chloromethyl ketone (TPCK)-treated trypsin, camostat, nafamostat, aprotinin and leupeptin. Chloromethylketone, E64-d and CA-074Me were from Enzo.

Viruses

The four human influenza virus strains and their abbreviations used in the text and figures are: A/Virginia/ATCC3/2009 (Virg09; A/H1N1 subtype; ATCC #VR-1737); A/HK/2/68

(HK68; A/H3N2 subtype) and B/Ned/537/05 (Ned05; B/Yamagata (B/Yam) lineage), both generously donated by R. Fouchier (Rotterdam, The Netherlands); and B/Malaysia/2506/04 (Mal04; B/Victoria (B/Vic) lineage; BEI resources #NR-12280). Viruses were expanded in 10-day old embryonated chicken eggs. For virus titration, a virus dilution series was added in quadruplo to Calu-3 cells. At day 3 post infection (p.i.), virus positivity was assessed by immunostaining for viral nucleoprotein (NP) (see below). Virus titers were expressed as the 50% cell culture infective dose ($CCID_{50}$), calculated by the method of Reed and Muench (88).

Plasmids

The panel of thirty-five pcDNA3.1+/C-(K)DYK plasmids containing the coding sequences for the 18 TTSPs, 16 KLKs and furin (for accession numbers and Clone IDs, see Table S1), was purchased from GenScript. The length of the ORFs was checked by PCR (Fig. S1). Expression of the different proteases was verified at 48 h post transfection of HEK293T cells, using dot blot assay. Cell lysates, prepared in RIPA buffer, were spotted onto a nitrocellulose membrane. The membrane was dried, blocked with 5% low fat milk powder in PBS, and incubated for 1 h with horseradish peroxidase (HRP)-conjugated anti-FLAG antibody (see full list of antibodies in Table S2). The dots were detected using SuperSignal™ West Femto Maximum Sensitivity Substrate (Thermo Fisher Scientific) and the ChemiDoc XRS+ System (Bio-Rad).

The expression plasmid for canine TMPRSS4 was constructed by extracting total RNA from MDCK cells, followed by reverse transcription and high-fidelity PCR using primers extended with EcoRV and XbaI sites, to allow subcloning into the pCAGEN vector provided by C. Cepko (Boston, MA) via Addgene (plasmid #11160). A similar cloning

procedure was used to prepare pCAGEN vectors with the HA and neuraminidase (NA) coding sequences from Virg09, HK68, Ned05 and Mal04, starting from allantoic virus stocks. These HA proteins were >99% identical to the following GenBank sequences published on NCBI (www.ncbi.nlm.nih.gov): AGI54750.1 (for Virg09); AFG71887.1 (for HK68); AGX16237.1 (for Ned05) and CY040449.1 (for Mal04).

The coding sequences for the A/H1 HA from A/South Carolina/1/1918 (SC1918) (GenBank: AF117241.1) and the N248D-mutant form of Mal04 HA were ordered from IDT. The cDNAs for A/H5 HA (ACA47835.1) from A/duck/Hunan/795/2002 (Hunan02); and the A/H7 HA (EPI439507) and A/N9 NA (EPI439509) from A/Anhui/1/2013 (Anhui13) were purchased from Sino Biological. cDNAs were amplified by Platinum™ SuperFi™ PCR (Invitrogen) and subcloned in the pCAGEN expression vector as described above. A/H1 HA from A/PR/8/34 (PR8; Sequence ID: AYA81842.1) was subcloned into pCAGEN starting from a pVP-HA reverse genetics plasmid, kindly donated by Dr. M. Kim (Daejeon, Korea).

Protease gene expression analysis in cells and human lung tissue

Lung tissue samples from eight different healthy donors were used. Calu-3, 16HBE, A549 and HEK293T lysates were made from three different cell passages. Total RNA was extracted using the ReliaPrep™ RNA Cell Miniprep System (Promega) and 0.5 µg RNA was converted to cDNA with the High-Capacity cDNA Reverse Transcription Kit (Thermo Fisher Scientific). BRYT Green™ dye-based quantitative PCR (qPCR) was performed with the GoTaq™ qPCR Master Mix (Promega) and intron-spanning primer pairs (see Table S3 for a list of all primers), in an ABI 7500 Fast Real-Time PCR system (Applied Biosciences). Expression data were normalized to the geometric mean of three

housekeeping genes (*GAPDH, HMBS, ACTB*) and analyzed using the $2^{-\Delta CT}$ method. All primers were checked for PCR efficiency and specificity by melt curve analysis. Microarray data for 108 healthy lung samples were obtained from GEO dataset GSE47460 (www.ncbi.nlm.nih.gov/geo) (89).

Western blot assay to monitor HA0 cleavage or HA protein expression

To assess HA0 cleavage in protease-expressing cells, HEK293T cells were seeded in growth medium at 300,000 cells per well in 12-well plates, and transfected with 0.5 µg pCAGEN-HA plasmid and 0.5 µg pcDNA3.1+/C-(K)DYK-protease plasmid, using Lipofectamine 2000 (Life Technologies). Four hours later, the growth medium was replaced by medium with 0.2% FCS and cells were further incubated at 37°C or 33°C (for B/Vic HA). At 48 h post transfection, the control well was exposed to 5 µg/ml TPCK-treated trypsin for 15 min at 37°C. Cells were then lysed in RIPA buffer supplemented with protease inhibitor cocktail (both from Thermo Fisher Scientific). The lysates were boiled for 5 min in 1X XT sample buffer containing 1X XT reducing agent (both from Bio-Rad) and resolved on 4-12% Bis-Tris XT Precast 26-well gels (Bio-Rad). Proteins were transferred to polyvinylidene difluoride membranes (Bio-Rad), blocked with 5% low fat milk powder, and probed for 1 h with primary antibody followed by 45 min with HRP-conjugated secondary antibody. Clathrin served as the loading control (Table S2 for a list of all antibodies). The bands were detected and visualized as explained above for the dot blot assay. To quantify HA protein expression at different temperatures, HEK293T or HeLa cells seeded in 12-well plates were transfected with pCAGEN-HA plasmid, incubated during 48 h at 33, 35, 37 or 39 °C, then exposed to exogenous trypsin when indicated. Cell extraction and western blot analysis were carried out as above.

Polykaryon assay to measure protease-mediated activation of HA or its fusion pH

The method was adapted from Vanderlinden *et al.* (90) to enable high-throughput format with high-content imaging. HeLa cells in black 96-well plates (20,000 cells per well) were reverse transfected with 50 ng pCAGEN-HA plasmid and 12.5 ng pcDNA3.1+/C-(K)DYK protease-plasmid using Fugene 6 (Promega). After 24 h, the growth medium was replaced by medium with 0.2% FCS and cells were further incubated at 37°C or 33°C (for B/Vic HA). Another 24 h later, the control conditions (which received HA plasmid only) were exposed for 15 min to MEM containing 5 µg/ml TPCK-treated trypsin. After gentle washing with PBS plus Ca^{2+} and Mg^{2+} (PBS-CM), the cells were exposed for 15 min to PBS-CM that had been pH-adjusted with citric acid to the required pH (i.e. a pH 0.1 unit lower than the fusion pH of that HA). After this pulse, the acidic PBS-CM was removed and growth medium with 10% FCS was added to stop the reaction. The cells were allowed to fuse during 4 h at 37°C (33°C for B/Vic HA, or another temperature if specifically mentioned), then fixated with 4% paraformaldehyde in PBS (15 min), permeabilized with 0.1% Triton X-100 (15 min) and stained for 30 min with 2 µg/ml HCS Cell Mask stain (Life Technologies). The plates were imaged using the CellInsight™ CX5 High Content Imaging Platform (Thermo Scientific). Nine images were taken per well and polykaryons were identified and counted using the SpotDetector protocol of the HCI software.

To determine the fusion pH of the different HAs, HeLa cells were transfected with the pCAGEN-HA plasmids and HA0 was cleaved with exogenous trypsin as above. During the acidic pulse, a range of acidic buffers was used having a pH between 4.9 to 6.0 with 0.1 increments. High-content imaging-based quantification of polykaryons was done as above. The fusion pH was defined as the pH at which the number of polykaryons was 50% of the maximum number (90).

Production of protease-activated HA pseudoparticles and transduction experiments

The method to produce fLuc-expressing retroviral vectors pseudotyped with a viral glycoprotein was previously described (91). In brief, HEK293T cells were transfected in 6-well plates, using calcium phosphate precipitation, with a mixture of plasmids encoding: MLV gag-pol (1.5 µg); an MLV vector coding for fLuc (3 µg); HA- and NA-expression plasmids (both 0.75 µg); plus the protease expression plasmids specified above (0.125 µg). The two additional expression vectors pCAGGS-HAT and pCAGGS-DESC1 were described before (71). At 16 h post transfection, the medium was replaced by medium with 2% FCS. At 48 h, the pseudoparticle-containing supernatants were harvested and clarified by centrifugation. To verify that all TTSP conditions contained a similar total number of pseudoparticles, they were subsequently exposed to trypsin. Namely, one half of the supernatant was left untreated and the other half was treated with 20 µg/ml trypsin for 15 min at 37°C, after which 20 µg/ml soybean trypsin inhibitor was added. To measure particle infectivity, HEK293T target cells were seeded in 96-well plates at a density of 20,000 cells per well. One day later, the cells were exposed to 100 µl virus stock, and 6 h later, fresh medium was added. To measure fLuc activity at day 3 post transduction, the cells were lysed for 10 min in 50 µl cold PBS with 0.5% Triton-X. The lysates were transferred to a white, opaque-walled 96-well plate and, after adding fLuc substrate (Beetle-Juice (PJK) kit), the signal was read in a microplate reader (Plate Chameleon V; Hidex) using MicroWin2000 software (version 4.44; Mikrotek Laborsysteme GmbH).

Virus replication following siRNA-mediated protease knockdown or exposure to trypsin

ON-TARGET*plus* siRNA SMARTpools targeting the thirty-five human proteases and a non-targeting (scrambled) control were ordered from Dharmacon (for catalogue numbers see Table S4). siRNAs targeting canine TMPRSS4 and canine ST14/matriptase were custom-synthesized by IDT (see sequences provided in Table S4). Cells suspended in a black 96-well plate (Calu-3: 35,000 cells per well, MDCK: 7,500 cells per well) were reverse transfected with 10 nM siRNA (each condition in quadruplo) using Lipofectamine RNAiMAX Transfection Reagent (Thermo Fisher Scientific). One day later, the transfection medium with 10% FCS was replaced by medium containing 0.2% FCS. Another 24 h later, the cells were infected with Virg09, HK68, Ned05 or Mal04 virus at a multiplicity of infection (MOI) of 100 $CCID_{50}$. At 72 h p.i., immunostaining for viral NP was performed. The cells were fixated for 5 min in 2% paraformaldehyde, permeabilized for 10 min with 0.1% Triton X-100, and blocked for 4 h in 1% bovine serum albumin (BSA). Next, the plates were stained overnight at 4°C with anti-NP antibody diluted in 1% BSA (for IAV: Hytest #3IN5 at 1/2000 and for IBV: Hytest #RIF17 at 1/2000). After washing in PBS containing 0.01% Tween, Alexa Fluor™ 488 secondary antibody (Invitrogen #A21424 at 1/500) was applied for 1 h at room temperature. Cell nuclei were stained with Hoechst (Thermo Fisher Scientific). The plates were imaged using the high-content platform specified above. Nine images per well were analyzed to determine the total (Hoechst) and infected (NP) cell numbers.

To measure their potential cytotoxic effects, the siRNAs were added to a parallel plate containing mock-infected cells. After five days incubation, cell viability was measured by the colorimetric MTS assay (CellTiter 96 AQ_{ueous} MTS Reagent from Promega) (92).

To quantify virus replication in the absence or presence of trypsin, the Calu-3 or MDCK cells were infected with virus as above, using infection medium with or without 2 µg/ml TPCK-treated trypsin, and 0.2% FCS. After 3 days incubation, the infection rate was determined by NP-staining and high-content imaging.

Data analysis

Unless stated otherwise, data shown are the mean ± SEM of three independent experiments. Graphpad Prism software (version 7.0) was used to analyze the data and construct the graphs. One-way ANOVA or Kruskal-Wallis with post hoc test for multiple comparisons was performed to compare groups as indicated in the figure legends. To compare two groups, the unpaired Student's t-test was used. *P*-values in the text and graphs are shown as: *≤ 0.05; **≤ 0.01, ***≤ 0.001; ****≤ 0.0001.

Acknowledgements

Part of this research work was performed using the 'Caps-It' research infrastructure (project ZW13-02) that was financially supported by the Hercules Foundation (FWO) and Rega Foundation, KU Leuven. The authors wish to thank John McDonough for assisting the GEO expression analysis; Dirk Daelemans for providing the high-content imaging infrastructure; and Wim van Dam for technical assistance.

References

1. World Health Organization. 2018. Influenza (seasonal) - Fact sheet No. 211. http://www.who.int/mediacentre/factsheets/fs211/en/. Accessed 12/03/2018.
2. Iuliano AD, Roguski KM, Chang HH, Muscatello DJ, Palekar R, Tempia S, Cohen C, Gran JM, Schanzer D, Cowling BJ, Wu P, Kyncl J, Ang LW, Park M, Redlberger-Fritz M, Yu H, Espenhain L, Krishnan A, Emukule G, van Asten L, Pereira da Silva S, Aungkulanon S, Buchholz U, Widdowson MA, Bresee JS. 2018. Estimates of global seasonal influenza-associated respiratory mortality: a modelling study. Lancet 391:1285-1300.
3. Glezen PW, Schmier JK, Kuehn CM, Ryan KJ, Oxford J. 2013. The burden of influenza B: a structured literature review. Am J Public Health 103:e43-51.
4. Nielsen J, Vestergaard LS, Richter L, Schmid D, Bustos N, Asikainen T, Trebbien R, Denissov G, Innos K, Virtanen MJ, Fouillet A, Lytras T, Gkolfinopoulou K, Heiden MA, Grabenhenrich L, Uphoff H, Paldy A, Bobvos J, Domegan L, O'Donnell J, Scortichini M, de Martino A, Mossong J, England K, Melillo J, van Asten L, de Lange MM, Tonnessen R, White RA, da Silva SP, Rodrigues AP, Larrauri A, Mazagatos C, Farah A, Carnahan AD, Junker C, Sinnathamby M, Pebody RG, Andrews N, Reynolds A, McMenamin J, Brown CS, Adlhoch C, Penttinen P, Molbak K, Krause TG. 2019. European all-cause excess and influenza-attributable mortality in the 2017/18 season: should the burden of influenza B be reconsidered? Clin Microbiol Infect doi:10.1016/j.cmi.2019.02.011.
5. Matias G, Taylor R, Haguinet F, Schuck-Paim C, Lustig R, Shinde V. 2014. Estimates of mortality attributable to influenza and RSV in the United States during 1997-2009 by influenza type or subtype, age, cause of death, and risk status. Influenza Other Respir Viruses 8:507-15.

6. Suzuki Y, Nei M. 2002. Origin and evolution of influenza virus hemagglutinin genes. Mol Biol Evol 19:501-9.

7. Vijaykrishna D, Holmes EC, Joseph U, Fourment M, Su YC, Halpin R, Lee RT, Deng YM, Gunalan V, Lin X, Stockwell TB, Fedorova NB, Zhou B, Spirason N, Kuhnert D, Boskova V, Stadler T, Costa AM, Dwyer DE, Huang QS, Jennings LC, Rawlinson W, Sullivan SG, Hurt AC, Maurer-Stroh S, Wentworth DE, Smith GJ, Barr IG. 2015. The contrasting phylodynamics of human influenza B viruses. Elife 4:e05055.

8. Long JS, Mistry B, Haslam SM, Barclay WS. 2018. Host and viral determinants of influenza A virus species specificity. Nat Rev Microbiol 17:67-81.

9. Koutsakos M, Nguyen TH, Barclay WS, Kedzierska K. 2016. Knowns and unknowns of influenza B viruses. Future Microbiol 11:119-35.

10. Osterhaus AD, Rimmelzwaan GF, Martina BE, Bestebroer TM, Fouchier RA. 2000. Influenza B virus in seals. Science 288:1051-3.

11. Long JS, Mistry B, Haslam SM, Barclay WS. 2019. Host and viral determinants of influenza A virus species specificity. Nature Reviews Microbiology 17:67-81.

12. Byrd-Leotis L, Cummings RD, Steinhauer DA. 2017. The interplay between the host receptor and influenza virus hemagglutinin and neuraminidase. Int J Mol Sci 18:1541.

13. Cross KJ, Burleigh LM, Steinhauer DA. 2001. Mechanisms of cell entry by influenza virus. Expert Rev Mol Med 3:1-18.

14. Das DK, Govindan R, Nikic-Spiegel I, Krammer F, Lemke EA, Munro JB. 2018. Direct visualization of the conformational dynamics of single influenza hemagglutinin trimers. Cell 174:1-12.

15. Klenk HD, Rott R, Orlich M, Blödorn J. 1975. Activation of influenza A viruses by trypsin treatment. Virology 68:426-439.

16. Laporte M, Naesens L. 2017. Airway proteases: an emerging drug target for influenza and other respiratory virus infections. Curr Opin Virol 24:16-24.

17. Böttcher-Friebertshäuser E, Lu Y, Meyer D, Sielaff F, Steinmetzer T, Klenk HD, Garten W. 2012. Hemagglutinin activating host cell proteases provide promising drug targets for the treatment of influenza A and B virus infections. Vaccine 30:7374-80.

18. Galloway SE, Liang B, Steinhauer DA. 2018. Activation of the hemagglutinin of influenza viruses, p 3-26. *In* Böttcher-Friebertshäuser E, Garten W, Klenk HD (ed), Activation of Viruses by Host Proteases doi:10.1007/978-3-319-75474-1. Springer International Publishing AG, Cham, Switzerland.

19. Hatesuer B, Bertram S, Mehnert N, Bahgat MM, Nelson PS, Pöhlmann S, Schughart K. 2013. Tmprss2 is essential for influenza H1N1 virus pathogenesis in mice. PLoS Pathog 9:e1003774.

20. Tarnow C, Engels G, Arendt A, Schwalm F, Sediri H, Preuss A, Nelson PS, Garten W, Klenk HD, Gabriel G, Böttcher-Friebertshäuser E. 2014. TMPRSS2 is a host factor that is essential for pneumotropism and pathogenicity of H7N9 influenza A virus in mice. J Virol 88:4744-51.

21. Sakai K, Ami Y, Tahara M, Kubota T, Anraku M, Abe M, Nakajima N, Sekizuka T, Shirato K, Suzaki Y, Ainai A, Nakatsu Y, Kanou K, Nakamura K, Suzuki T, Komase K, Nobusawa E, Maenaka K, Kuroda M, Hasegawa H, Kawaoka Y, Tashiro M, Takeda M. 2014. The host protease TMPRSS2 plays a major role in in vivo replication of emerging H7N9 and seasonal influenza viruses. J Virol 88:5608-16.

22. Lambertz RLO, Gerhauser I, Nehlmeier I, Leist SR, Kollmus H, Pohlmann S, Schughart K. 2019. Tmprss2 knock-out mice are resistant to H10 influenza A virus pathogenesis. J Gen Virol doi:10.1099/jgv.0.001274.

23. Cheng Z, Zhou J, To KK, Chu H, Li C, Wang D, Yang D, Zheng S, Hao K, Bosse Y, Obeidat M, Brandsma CA, Song YQ, Chen Y, Zheng BJ, Li L, Yuen KY. 2015. Identification of TMPRSS2 as a susceptibility gene for severe 2009 pandemic A(H1N1) influenza and A(H7N9) influenza. J Infect Dis 212:1214-21.

24. Hamilton BS, Whittaker GR, Daniel S. 2012. Influenza virus-mediated membrane fusion: determinants of hemagglutinin fusogenic activity and experimental approaches for assessing virus fusion. Viruses 4:1144-68.

25. Limburg H, Harbig A, Bestle D, Stein DA, Moulton HM, Jaeger J, Janga H, Hardes K, Koepke J, Schulte L, Koczulla AR, Schmeck B, Klenk HD, Böttcher-Friebertshäuser E. 2019. TMPRSS2 is the major activating protease of influenza A virus in primary human airway cells and influenza B virus in human type II pneumocytes. J Virol doi:10.1128/jvi.00649-19.

26. Sakai K, Ami Y, Nakajima N, Nakajima K, Kitazawa M, Anraku M, Takayama I, Sangsriratanakul N, Komura M, Sato Y, Asanuma H, Takashita E, Komase K, Takehara K, Tashiro M, Hasegawa H, Odagiri T, Takeda M. 2016. TMPRSS2 independency for haemagglutinin cleavage in vivo differentiates influenza B virus from Iinfluenza A virus. Sci Rep 6:29430.

27. Russell CJ, Hu M, Okda FA. 2018. Influenza hemagglutinin protein stability, activation, and pandemic risk. Trends Microbiol 26:841-853.

28. Singanayagam A, Zambon M, Barclay W. 2019. Influenza virus with increased pH of HA activation has improved replication in cell culture but at the cost of infectivity in human airway epithelium. J Virol doi:10.1128/JVI.00058-19.

29. Fischer H, Widdicombe JH. 2006. Mechanisms of acid and base secretion by the airway epithelium. J Membr Biol 211:139-50.

30. England RJ, Homer JJ, Knight LC, Ell SR. 1999. Nasal pH measurement: a reliable and repeatable parameter. Clin Otolaryngol Allied Sci 24:67-8.

31. Russier M, Yang G, Rehg JE, Wong SS, Mostafa HH, Fabrizio TP, Barman S, Krauss S, Webster RG, Webby RJ, Russell CJ. 2016. Molecular requirements for a pandemic influenza virus: An acid-stable hemagglutinin protein. Proc Natl Acad Sci U S A 113:1636-41.

32. Baumann J, Kouassi NM, Foni E, Klenk HD, Matrosovich M. 2016. H1N1 swine influenza viruses differ from avian precursors by a higher pH optimum of membrane fusion. J Virol 90:1569-77.

33. Imai M, Watanabe T, Hatta M, Das SC, Ozawa M, Shinya K, Zhong G, Hanson A, Katsura H, Watanabe S, Li C, Kawakami E, Yamada S, Kiso M, Suzuki Y, Maher EA, Neumann G, Kawaoka Y. 2012. Experimental adaptation of an influenza H5 HA confers respiratory droplet transmission to a reassortant H5 HA/H1N1 virus in ferrets. Nature 486:420-8.

34. Linster M, van Boheemen S, de Graaf M, Schrauwen EJA, Lexmond P, Manz B, Bestebroer TM, Baumann J, van Riel D, Rimmelzwaan GF, Osterhaus A, Matrosovich M, Fouchier RAM, Herfst S. 2014. Identification, characterization, and natural selection of mutations driving airborne transmission of A/H5N1 virus. Cell 157:329-339.

35. Lindemann J, Leiacker R, Rettinger G, Keck T. 2002. Nasal mucosal temperature during respiration. Clin Otolaryngol Allied Sci 27:135-9.

36. McFadden ER, Jr., Pichurko BM, Bowman HF, Ingenito E, Burns S, Dowling N, Solway J. 1985. Thermal mapping of the airways in humans. J Appl Physiol 58:564-70.

37. Aggarwal S, Dewhurst S, Takimoto T, Kim B. 2011. Biochemical impact of the host adaptation-associated PB2 E627K mutation on the temperature-dependent RNA synthesis kinetics of influenza A virus polymerase complex. J Biol Chem 286:34504-13.

38. Scull MA, Gillim-Ross L, Santos C, Roberts KL, Bordonali E, Subbarao K, Barclay WS, Pickles RJ. 2009. Avian Influenza virus glycoproteins restrict virus replication and spread through human airway epithelium at temperatures of the proximal airways. PLoS Pathog 5:e1000424.

39. Ohler A, Becker-Pauly C. 2012. TMPRSS4 is a type II transmembrane serine protease involved in cancer and viral infections. Biol Chem 393:907-14.

40. Kalinska M, Meyer-Hoffert U, Kantyka T, Potempa J. 2016. Kallikreins - The melting pot of activity and function. Biochimie 122:270-82.

41. Klenk H-D, Garten W. 1994. Host cell proteases controlling virus pathogenicity. Trends in Microbiology 2.

42. Bertram S, Glowacka I, Blazejewska P, Soilleux E, Allen P, Danisch S, Steffen I, Choi SY, Park Y, Schneider H, Schughart K, Pöhlmann S. 2010. TMPRSS2 and TMPRSS4 facilitate trypsin-independent spread of influenza virus in Caco-2 cells. J Virol 84:10016-25.

43. Galloway SE, Reed ML, Russell CJ, Steinhauer DA. 2013. Influenza HA subtypes demonstrate divergent phenotypes for cleavage activation and pH of fusion: implications for host range and adaptation. PLoS Pathog 9:e1003151.

44. Gamblin SJ, Skehel JJ. 2010. Influenza hemagglutinin and neuraminidase membrane glycoproteins. J Biol Chem 285:28403-9.

45. Kobasa D, Takada A, Shinya K, Hatta M, Halfmann P, Theriault S, Suzuki H, Nishimura H, Mitamura K, Sugaya N, Usui T, Murata T, Maeda Y, Watanabe S, Suresh M, Suzuki T, Suzuki Y, Feldmann H, Kawaoka Y. 2004. Enhanced virulence of influenza A viruses with the haemagglutinin of the 1918 pandemic virus. Nature 431:703-707.

46. Watanabe T, Tisoncik-Go J, Tchitchek N, Watanabe S, Benecke AG, Katze MG, Kawaoka Y. 2013. 1918 Influenza virus hemagglutinin (HA) and the viral RNA polymerase complex enhance viral pathogenicity, but only HA induces aberrant host responses in mice. J Virol 87:5239-54.

47. Taubenberger JK, Morens DM. 2006. 1918 influenza: the mother of all pandemics. Emerging Infectious Diseases 12:15-22.

48. Short KR, Kedzierska K, van de Sandt CE. 2018. Back to the future: lessons learned from the 1918 influenza pandemic. Front Cell Infect Microbiol 8:343.

806 49. Quan C, Shi W, Yang Y, Yang Y, Liu X, Xu W, Li H, Li J, Wang Q, Tong Z, Wong G,
807 Zhang C, Ma S, Ma Z, Fu G, Zhang Z, Huang Y, Song H, Yang L, Liu WJ, Liu Y, Liu W,
808 Gao GF, Bi Y. 2018. New threats from H7N9 influenza virus: spread and evolution of
809 high- and low-pathogenicity variants with high genomic diversity in wave five. J Virol
810 92:e00301-18.
811 50. Chaipan C, Kobasa D, Bertram S, Glowacka I, Steffen I, Tsegaye TS, Takeda M, Bugge
812 TH, Kim S, Park Y, Marzi A, Pöhlmann S. 2009. Proteolytic activation of the 1918
813 influenza virus hemagglutinin. J Virol 83:3200-11.
814 51. Zhou Y, Vedantham P, Lu K, Agudelo J, Carrion R, Jr., Nunneley JW, Barnard D,
815 Pöhlmann S, McKerrow JH, Renslo AR, Simmons G. 2015. Protease inhibitors targeting
816 coronavirus and filovirus entry. Antiviral Res 116:76-84.
817 52. Noma K, Kiyotani K, Kouchi H, Fujii Y, Egi Y, Tanaka K, Yoshida T. 1998. Endogenous
818 protease-dependent replication of human influenza viruses in two MDCK cell lines. Arch
819 Virol 143:1893-909.
820 53. Tumpey TM, Basler CF, Aguilar PV, Zeng H, Solorzano A, Swayne DE, Cox NJ, Katz
821 JM, Taubenberger JK, Palese P, Garcia-Sastre A. 2005. Characterization of the
822 reconstructed 1918 Spanish influenza pandemic virus. Science 310:77-80.
823 54. Godiksen S, Selzer-Plon J, Pedersen ED, Abell K, Rasmussen HB, Szabo R, Bugge TH,
824 Vogel LK. 2008. Hepatocyte growth factor activator inhibitor-1 has a complex subcellular
825 itinerary. Biochem J 413:251-9.
826 55. Baron J, Tarnow C, Mayoli-Nussle D, Schilling E, Meyer D, Hammami M, Schwalm F,
827 Steinmetzer T, Guan Y, Garten W, Klenk HD, Böttcher-Friebertshäuser E. 2013.
828 Matriptase, HAT, and TMPRSS2 activate the hemagglutinin of H9N2 influenza A viruses.
829 J Virol 87:1811-20.
830 56. Lugovtsev VY, Melnyk D, Weir JP. 2013. Heterogeneity of the MDCK cell line and its
831 applicability for influenza virus research. PLoS One 8:e75014.

57. Hamilton BS, Gludish DW, Whittaker GR. 2012. Cleavage activation of the human-adapted influenza virus subtypes by matriptase reveals both subtype and strain specificities. J Virol 86:10579-86.

58. Beaulieu A, Gravel E, Cloutier A, Marois I, Colombo E, Desilets A, Verreault C, Leduc R, Marsault E, Richter MV. 2013. Matriptase proteolytically activates influenza virus and promotes multicycle replication in the human airway epithelium. J Virol 87:4237-51.

59. McShane D, Davies JC, Davies MG, Bush A, Geddes DM, Alton EW. 2003. Airway surface pH in subjects with cystic fibrosis. Eur Respir J 21:37-42.

60. Russell CJ. 2014. Acid-induced membrane fusion by the hemagglutinin protein and its role in influenza virus biology. Curr Top Microbiol Immunol 385:93-116.

61. Zaraket H, Bridges OA, Russell CJ. 2013. The pH of activation of the hemagglutinin protein regulates H5N1 influenza virus replication and pathogenesis in mice. J Virol 87:4826-34.

62. Zaraket H, Baranovich T, Kaplan BS, Carter R, Song MS, Paulson JC, Rehg JE, Bahl J, Crumpton JC, Seiler J, Edmonson M, Wu G, Karlsson E, Fabrizio T, Zhu H, Guan Y, Husain M, Schultz-Cherry S, Krauss S, McBride R, Webster RG, Govorkova EA, Zhang J, Russell CJ, Webby RJ. 2015. Mammalian adaptation of influenza A(H7N9) virus is limited by a narrow genetic bottleneck. Nat Commun 6:6553.

63. Mittal A, Shangguan T, Bentz J. 2002. Measuring pKa of Activation and pKi of Inactivation for Influenza Hemagglutinin from Kinetics of Membrane Fusion of Virions and of HA Expressing Cells. Biophys J 83:2652–2666.

64. Prinzinger R, Preßmar A, Schleucher E. 1991. Body temperature in birds. Comp Biochem Phys 99:499-506.

65. Massin P, van der Werf S, Naffakh N. 2001. Residue 627 of PB2 is a determinant of cold sensitivity in RNA replication of avian influenza viruses. J Virol 75:5398-404.

857 66. An Y, Cipollo JF. 2011. An unbiased approach for analysis of protein glycosylation and
858 application to influenza vaccine hemagglutinin. Anal Biochem 415:67-80.
859 67. Ni F, Kondrashkina E, Wang Q. 2013. Structural basis for the divergent evolution of
860 influenza B virus hemagglutinin. Virology 446:112-22.
861 68. Hamilton BS, Whittaker GR. 2013. Cleavage activation of human-adapted influenza virus
862 subtypes by kallikrein-related peptidases 5 and 12. J Biol Chem 288:17399-407.
863 69. Magnen M, Elsasser BM, Zbodakova O, Kasparek P, Gueugnon F, Petit-Courty A,
864 Sedlacek R, Goettig P, Courty Y. 2018. Kallikrein-related peptidase 5 and seasonal
865 influenza viruses, limitations of the experimental models for activating proteases. Biol
866 Chem 399:1053-1064.
867 70. Garten W, Braden C, Arendt A, Peitsch C, Baron J, Lu Y, Pawletko K, Hardes K,
868 Steinmetzer T, Böttcher-Friebertshäuser E. 2015. Influenza virus activating host
869 proteases: identification, localization and inhibitors as potential therapeutics. Eur J Cell
870 Biol 94:375-83.
871 71. Zmora P, Blazejewska P, Moldenhauer AS, Welsch K, Nehlmeier I, Wu Q, Schneider H,
872 Pöhlmann S, Bertram S. 2014. DESC1 and MSPL activate influenza A viruses and
873 emerging coronaviruses for host cell entry. J Virol 88:12087-97.
874 72. Zhirnov OP, Manykin AA, Rossman JS, Klenk HD. 2016. Intravirion cohesion of matrix
875 protein M1 with ribonucleocapsid is a prerequisite of influenza virus infectivity. Virology
876 492:187-96.
877 73. Hebert DN, Zhang JX, Chen W, Foellmer B, Helenius A. 1997. The number and location
878 of glycans on influenza hemagglutinin determine folding and association with calnexin
879 and calreticulin. J Cell Biol 139:613-23.
880 74. Sakai K, Sekizuka T, Ami Y, Nakajima N, Kitazawa M, Sato Y, Nakajima K, Anraku M,
881 Kubota T, Komase K, Takehara K, Hasegawa H, Odagiri T, Tashiro M, Kuroda M,
882 Takeda M. 2015. A mutant H3N2 influenza virus uses an alternative activation

mechanism in TMPRSS2 knockout mice by loss of an oligosaccharide in the hemagglutinin stalk region. J Virol 89:5154-8.

75. Chen J, Lee KH, Steinhauer DA, Stevens DJ, Skehel JJ, Wiley DC. 1998. Structure of the hemagglutinin precursor cleavage site, a determinant of influenza pathogenicity and the origin of the labile conformation. Cell 95:409-17.

76. Stevens J, Corper AL, Basler CF, Taubenberger JK, Palese P, Wilson IA. 2004. Structure of the uncleaved human H1 hemagglutinin from the extinct 1918 influenza virus. Science 303:1866-70.

77. Brassard DL, Lamb RA. 1997. Expression of influenza B virus hemagglutinin containing multibasic residue cleavage sites. Virology 236:234-48.

78. Nakowitsch S, Waltenberger AM, Wressnigg N, Ferstl N, Triendl A, Kiefmann B, Montomoli E, Lapini G, Sergeeva M, Muster T, Romanova JR. 2014. Egg- or cell culture-derived hemagglutinin mutations impair virus stability and antigen content of inactivated influenza vaccines. Biotechnol J 9:405-14.

79. Takashita E, Muraki Y, Sugawara K, Asao H, Nishimura H, Suzuki K, Tsuji T, Hongo S, Ohara Y, Kawaoka Y, Ozawa M, Matsuzaki Y. 2012. Intrinsic temperature sensitivity of influenza C virus hemagglutinin-esterase-fusion protein. J Virol 86:13108-11.

80. Chen Z, Aspelund A, Kemble G, Jin H. 2008. Molecular studies of temperature-sensitive replication of the cold-adapted B/Ann Arbor/1/66, the master donor virus for live attenuated influenza FluMist vaccines. Virology 380:354-62.

81. Ueda M, Sugiura A. 1984. Physiological characterization of influenza virus temperature-sensitive mutants defective in the haemagglutinin gene. J Gen Virol 65 1889-97.

82. Schuy W, Will C, Kuroda K, Scholtissek C, Garten W, Klenk HD. 1986. Mutations blocking the transport of the influenza virus hemagglutinin between the rough endoplasmic reticulum and the Golgi apparatus. EMBO J 5:2831-6.

83. Gallagher PJ, Henneberry JM, Sambrook JF, Gething MJ. 1992. Glycosylation requirements for intracellular transport and function of the hemagglutinin of influenza virus. J Virol 66:7136-45.

84. Roberts PC, Garten W, Klenk HD. 1993. Role of conserved glycosylation sites in maturation and transport of influenza A virus hemagglutinin. J Virol 67:3048-60.

85. Gerlach T, Hensen L, Matrosovich T, Bergmann J, Winkler M, Peteranderl C, Klenk HD, Weber F, Herold S, Pohlmann S, Matrosovich M. 2017. pH Optimum of Hemagglutinin-Mediated Membrane Fusion Determines Sensitivity of Influenza A Viruses to the Interferon-Induced Antiviral State and IFITMs. J Virol 91:1-16.

86. Koerner I, Matrosovich MN, Haller O, Staeheli P, Kochs G. 2012. Altered receptor specificity and fusion activity of the haemagglutinin contribute to high virulence of a mouse-adapted influenza A virus. J Gen Virol 93:970-9.

87. Takahashi T, Kurebayashi Y, Ikeya K, Mizuno T, Fukushima K, Kawamoto H, Kawaoka Y, Suzuki Y, Suzuki T. 2010. The low-pH stability discovered in neuraminidase of 1918 pandemic influenza A virus enhances virus replication. PLoS One 5:e15556.

88. Reed LJ, Muench H. 1938. A simple method of estimating fifty per cent endpoints. Am J Epidemiol 27:493-497.

89. McDonough JE, Kaminski N, Thienpont B, Hogg JC, Vanaudenaerde BM, Wuyts WA. 2019. Gene correlation network analysis to identify regulatory factors in idiopathic pulmonary fibrosis. Thorax 74:132-140.

90. Vanderlinden E, Göktas F, Cesur Z, Froeyen M, Reed ML, Russell CJ, Cesur N, Naesens L. 2010. Novel inhibitors of influenza virus fusion: structure-activity relationship and interaction with the viral hemagglutinin. J Virol 84:4277-88.

91. Simmons G, Reeves JD, Grogan CC, Vandenberghe LH, Baribaud F, Whitbeck JC, Burke E, Buchmeier MJ, Soilleux EJ, Riley JL, Doms RW, Bates P, Pöhlmann S. 2003.

DC-SIGN and DC-SIGNR Bind Ebola Glycoproteins and Enhance Infection of Macrophages and Endothelial Cells. Virology 305:115-123.

92. Vrijens P, Noppen S, Boogaerts T, Vanstreels E, Ronca R, Chiodelli P, Laporte M, Vanderlinden E, Liekens S, Stevaert A, Naesens L. 2019. Influenza virus entry via the GM3 ganglioside-mediated platelet-derived growth factor receptor beta signalling pathway. J Gen Virol 100:583-601.

Figure 1

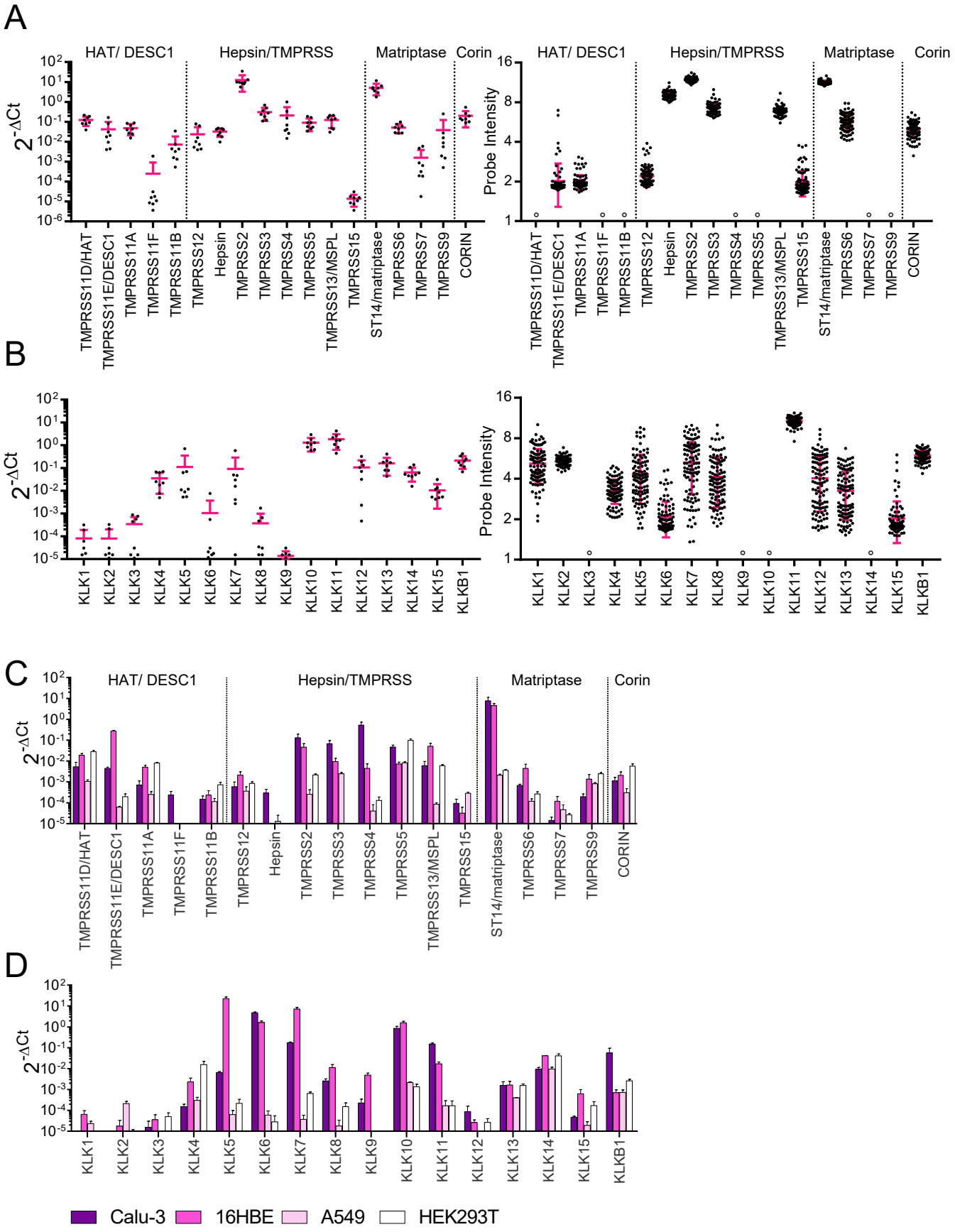
A
HAT/ DESC1
Hepsin/TMPRSS
Matriptase
Corin
$2^{-\Delta Ct}$
Probe Intensity
TMPRSS11D/HAT
TMPRSS11E/DESC1
TMPRSS11A
TMPRSS11F
TMPRSS11B
TMPRSS12
Hepsin
TMPRSS2
TMPRSS3
TMPRSS4
TMPRSS5
TMPRSS13/MSPL
TMPRSS15
ST14/matriptase
TMPRSS6
TMPRSS7
TMPRSS9
CORIN
B
KLK1
KLK2
KLK3
KLK4
KLK5
KLK6
KLK7
KLK8
KLK9
KLK10
KLK11
KLK12
KLK13
KLK14
KLK15
KLKB1
C
D
Calu-3
16HBE
A549
HEK293T

939 **Figure 1. Human lung tissue and airway epithelial cell lines are rich in TTSP and**

940 **KLK enzymes.**

941 (A) *TTSP* and (B) *KLK* transcript levels in healthy human lung, measured by RT-qPCR

942 on samples from eight different donors (left), or retrieved from the NCBI GEO database

943 (GEO dataset GSE47460) (right). Individual data points (in black) ± SEM (in pink). °No

944 data available. (C, D) Transcript levels in human airway epithelial Calu-3, 16HBE and

945 A549 cells, and human embryonic kidney HEK293T cells. The four TTSP subfamilies are

946 indicated at the top of the graphs.

Figure 2

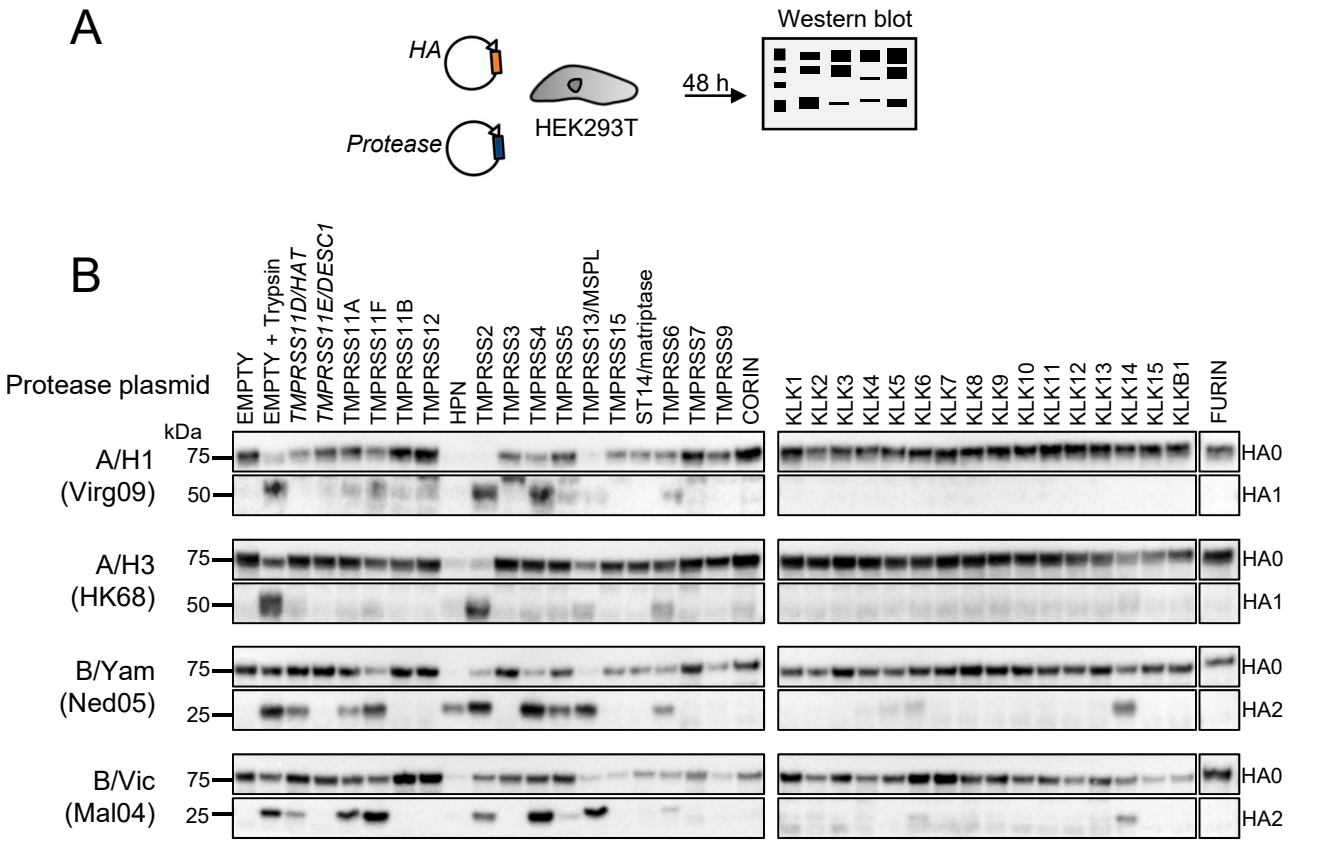
A
HA
Protease
HEK293T
48 h
Western blot
B
Protease plasmid
EMPTY
EMPTY + Trypsin
TMPRSS11D/HAT
TMPRSS11E/DESC1
TMPRSS11A
TMPRSS11F
TMPRSS11B
TMPRSS12
HPN
TMPRSS2
TMPRSS3
TMPRSS4
TMPRSS5
TMPRSS13/MSPL
TMPRSS15
ST14/matriptase
TMPRSS6
TMPRSS7
TMPRSS9
CORIN
KLK1
KLK2
KLK3
KLK4
KLK5
KLK6
KLK7
KLK8
KLK9
KLK10
KLK11
KLK12
KLK13
KLK14
KLK15
KLKB1
FURIN
kDa
A/H1 (Virg09)
A/H3 (HK68)
B/Yam (Ned05)
B/Vic (Mal04)
75
50
25
HA0
HA1
HA2

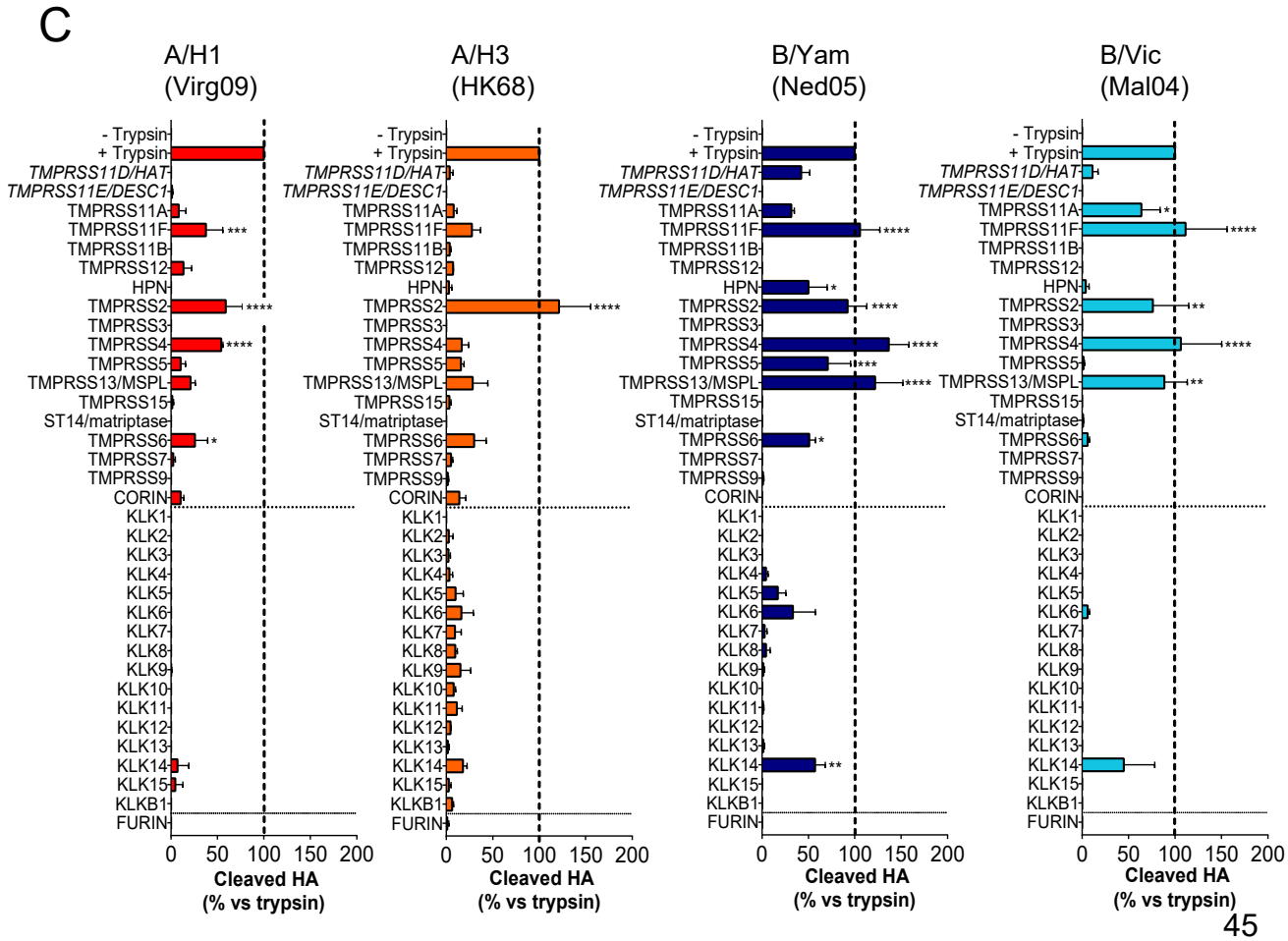
C
A/H1 (Virg09)
A/H3 (HK68)
B/Yam (Ned05)
B/Vic (Mal04)
- Trypsin
+ Trypsin
TMPRSS11D/HAT
TMPRSS11E/DESC1
TMPRSS11A
TMPRSS11F
TMPRSS11B
TMPRSS12
HPN
TMPRSS2
TMPRSS3
TMPRSS4
TMPRSS5
TMPRSS13/MSPL
TMPRSS15
ST14/matriptase
TMPRSS6
TMPRSS7
TMPRSS9
CORIN
KLK1
KLK2
KLK3
KLK4
KLK5
KLK6
KLK7
KLK8
KLK9
KLK10
KLK11
KLK12
KLK13
KLK14
KLK15
KLKB1
FURIN
0
50
100
150
200
Cleaved HA
(% vs trypsin)

947 **Figure 2. IBV HA0 is efficiently cleaved by a broad range of TTSPs.**

948 (A) Experiment set-up. HEK293T cells were transfected with two plasmids, one encoding
949 IAV or IBV HA and one encoding the indicated TTSP, KLK or furin. The HA cleavage state
950 was determined at 48 h post transfection. (B) Representative western blots showing the
951 bands of uncleaved HA0 and cleaved HA1 or HA2. The trypsin controls (second lanes on
952 each row), consisted of cells transfected with HA and a protease-lacking empty plasmid,
953 and exposed to trypsin for 15 min just before cell extraction. (C) Quantitative data for
954 TTSP- and KLK-mediated HA0 cleavage. For each HA, the intensity of the HA1 or HA2
955 band was normalized to clathrin and the % cleaved HA (mean ± SEM; N=3) was
956 expressed relative to the trypsin control. *P*-value *versus* no trypsin: *≤ 0.05; **≤ 0.01; ***≤
957 0.001; ****≤ 0.0001 (ordinary one-way ANOVA, followed by Dunnett's test).

Figure 3

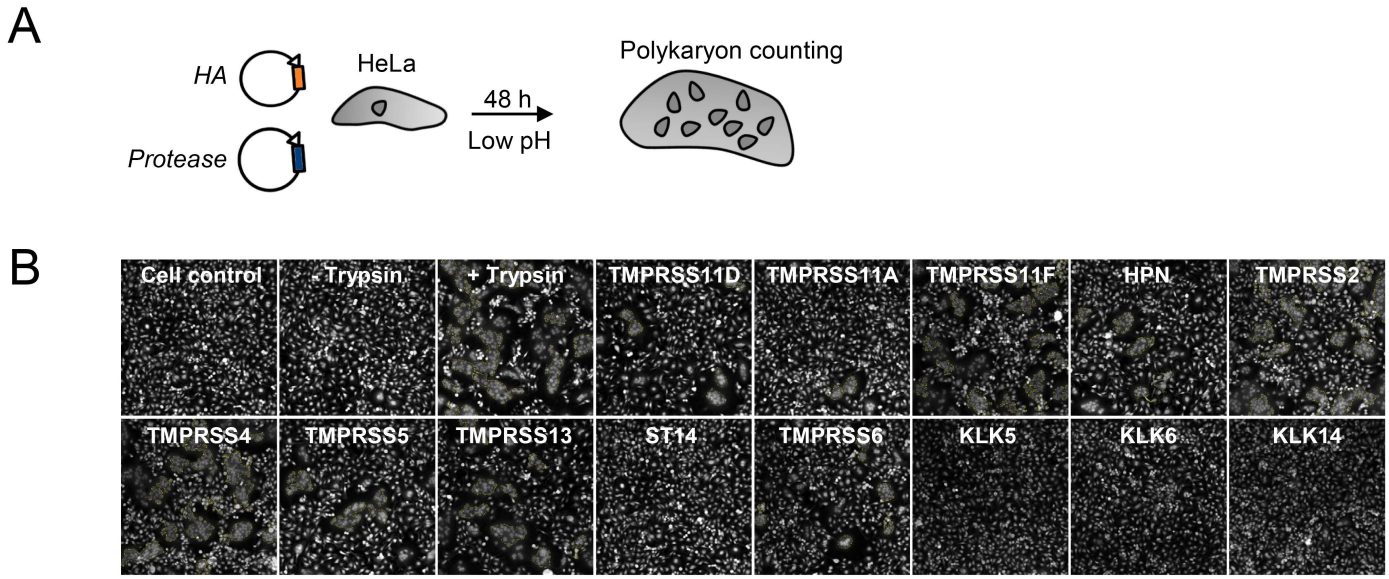

Figure 3. TTSP cleavage generates fusion-competent IBV HA.

(A) Experiment set-up. HeLa cells expressing IBV (B/Yam) HA plus a TTSP or KLK protease were exposed to an acidic buffer 0.1 units below the fusion pH.

(B) Representative photographs showing polykaryon formation in cells expressing IBV (B/Yam) HA. Polykaryon formation was similar in cells expressing B/Vic HA (not shown). The yellow contours show the polykaryons identified by high-content imaging software. The trypsin control (third photograph) received an empty (i.e. protease-lacking) plasmid and underwent HA activation by 15 min exposure to trypsin just before the acidic pulse.

Figure 4

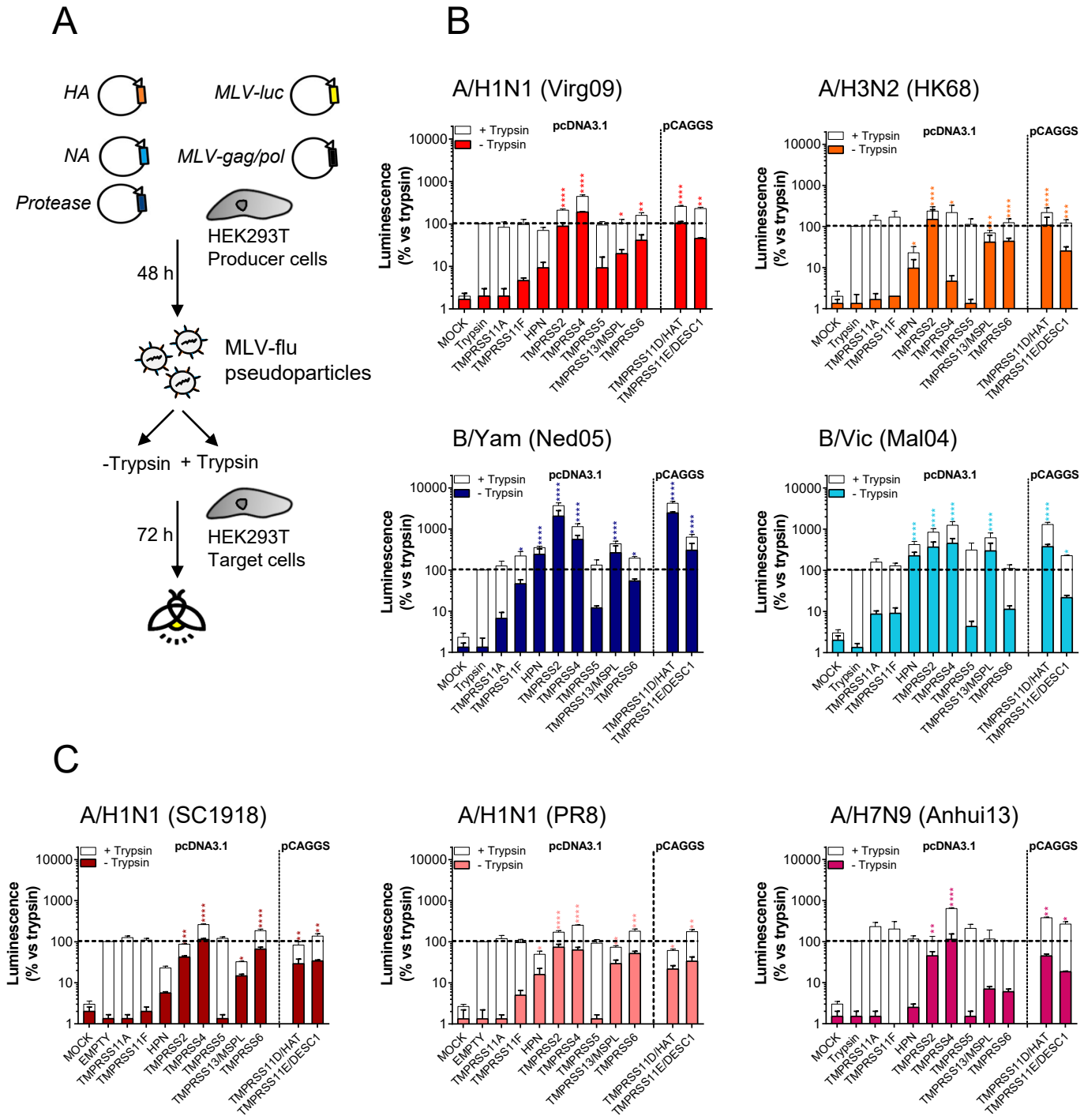
A
HA
MLV-luc
NA
MLV-gag/pol
Protease
HEK293T
Producer cells
48 h
MLV-flu
pseudoparticles
-Trypsin
+ Trypsin
72 h
HEK293T
Target cells
B
A/H1N1 (Virg09)
A/H3N2 (HK68)
B/Yam (Ned05)
B/Vic (Mal04)
C
A/H1N1 (SC1918)
A/H1N1 (PR8)
A/H7N9 (Anhui13)
+ Trypsin
- Trypsin
pcDNA3.1
pCAGGS
Luminescence
(% vs trypsin)
MOCK
EMPTY
Trypsin
TMPRSS11A
TMPRSS11F
HPN
TMPRSS2
TMPRSS4
TMPRSS5
TMPRSS13/MSPL
TMPRSS6
TMPRSS11D/HAT
TMPRSS11E/DESC1

966 **Figure 4. Pseudoparticles carrying IBV HA are efficiently activated by different**
967 **TTSPs.**
968 (A) Experiment set-up. HEK293T producer cells were transfected with plasmids encoding
969 the HA and NA from IAV or IBV, MLV-backbone, MLV-luciferase reporter and a TTSP
970 enzyme. The produced pseudoparticles were left untreated (to assess TTSP-induced
971 infectivity), or were secondarily treated with trypsin (to measure total particle infectivity).
972 After transducing HEK293T target cells, luminescence was measured at day 3 day p.i.
973 (B, C) Transduction efficiency (relative to the trypsin control) of TTSP-activated
974 pseudoparticles tested as such (in color) or after additional trypsin treatment (in white).
975 Data are the mean ± SEM (N=3 with triplicate read-outs). *P*-value *versus* no trypsin:
976 *≤ 0.05; ***≤ 0.001; ****≤ 0.0001 (Kruskall-Wallis, followed by Dunnett's test).

Figure 5

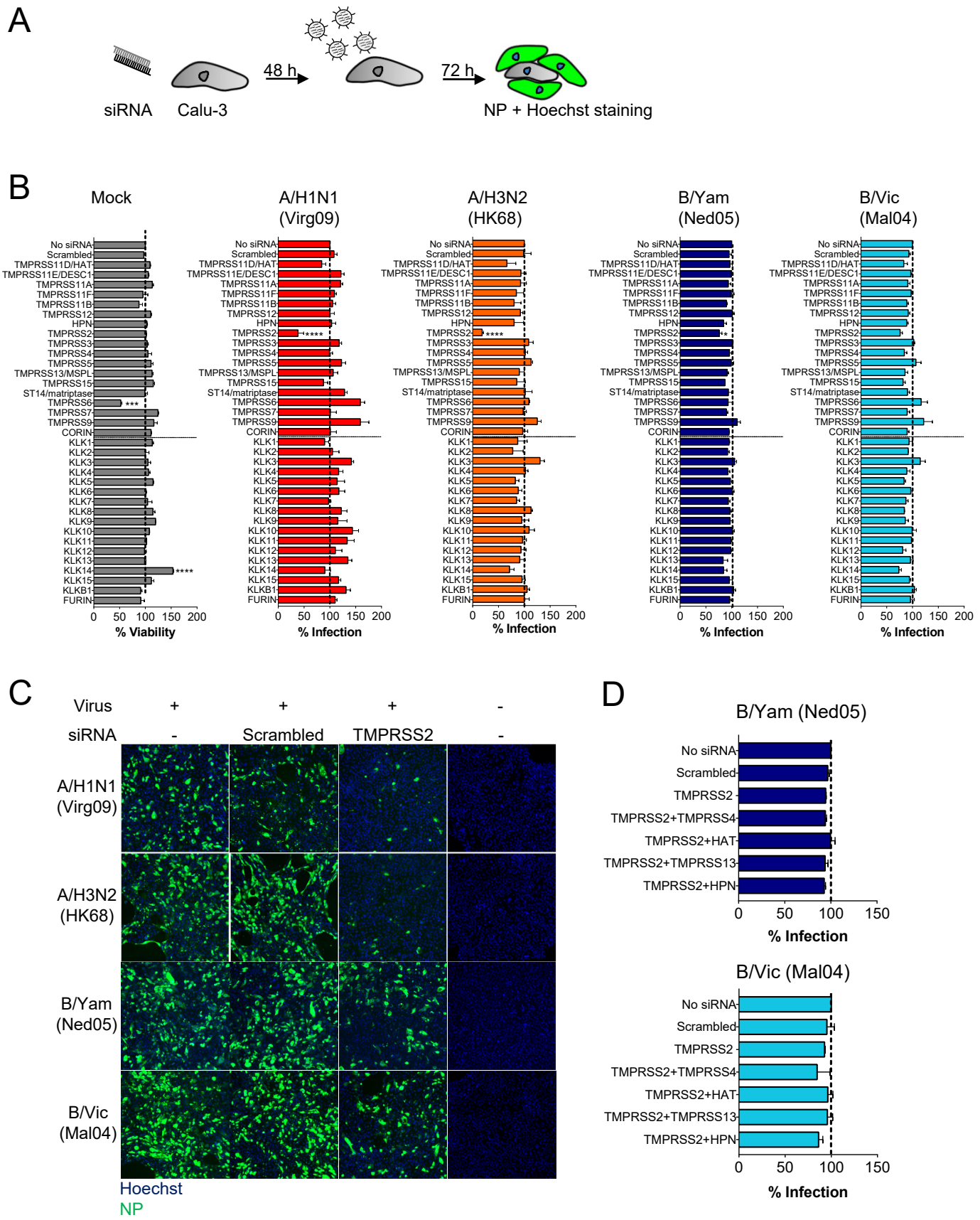
A
siRNA
Calu-3
48 h
72 h
NP + Hoechst staining
B
Mock
A/H1N1 (Virg09)
A/H3N2 (HK68)
B/Yam (Ned05)
B/Vic (Mal04)
No siRNA
Scrambled
TMPRSS11D/HAT
TMPRSS11E/DESC1
TMPRSS11A
TMPRSS11F
TMPRSS11B
TMPRSS12
HPN
TMPRSS2
TMPRSS3
TMPRSS4
TMPRSS5
TMPRSS13/MSPL
TMPRSS15
ST14/matriptase
TMPRSS6
TMPRSS7
TMPRSS9
CORIN
KLK1
KLK2
KLK3
KLK4
KLK5
KLK6
KLK7
KLK8
KLK9
KLK10
KLK11
KLK12
KLK13
KLK14
KLK15
KLKB1
FURIN
% Viability
% Infection
C
Virus + + + -
siRNA - Scrambled TMPRSS2 -
A/H1N1 (Virg09)
A/H3N2 (HK68)
B/Yam (Ned05)
B/Vic (Mal04)
Hoechst
NP
D
B/Yam (Ned05)
B/Vic (Mal04)
No siRNA
Scrambled
TMPRSS2
TMPRSS2+TMPRSS4
TMPRSS2+HAT
TMPRSS2+TMPRSS13
TMPRSS2+HPN
% Infection

977 **Figure 5. TMPRSS2 is a crucial protease for replication of IAV but not IBV.**

978 (A) Experiment set-up. Calu-3 cells were transfected with TTSP- or KLK-targeting siRNA
979 and infected with IAV or IBV. The % infected cells was quantified by high-content imaging
980 of NP. (B) Impact of protease knockdown on cell viability (grey bars) or virus growth
981 (colored bars), expressed relative to the condition receiving no siRNA. Data are the mean
982 ± SEM (N=3 with four replicates). *P*-value *versus* scrambled siRNA: *≤ 0.05; ***≤ 0.001;
983 ****≤ 0.0001 (ordinary one-way ANOVA, followed by Dunnett's test). (C) TMPRSS2
984 knockdown markedly reduces IAV but not IBV replication, as shown by NP-staining. (D)
985 IBV infection in Calu-3 cells receiving combinations of siRNAs.

Figure 6

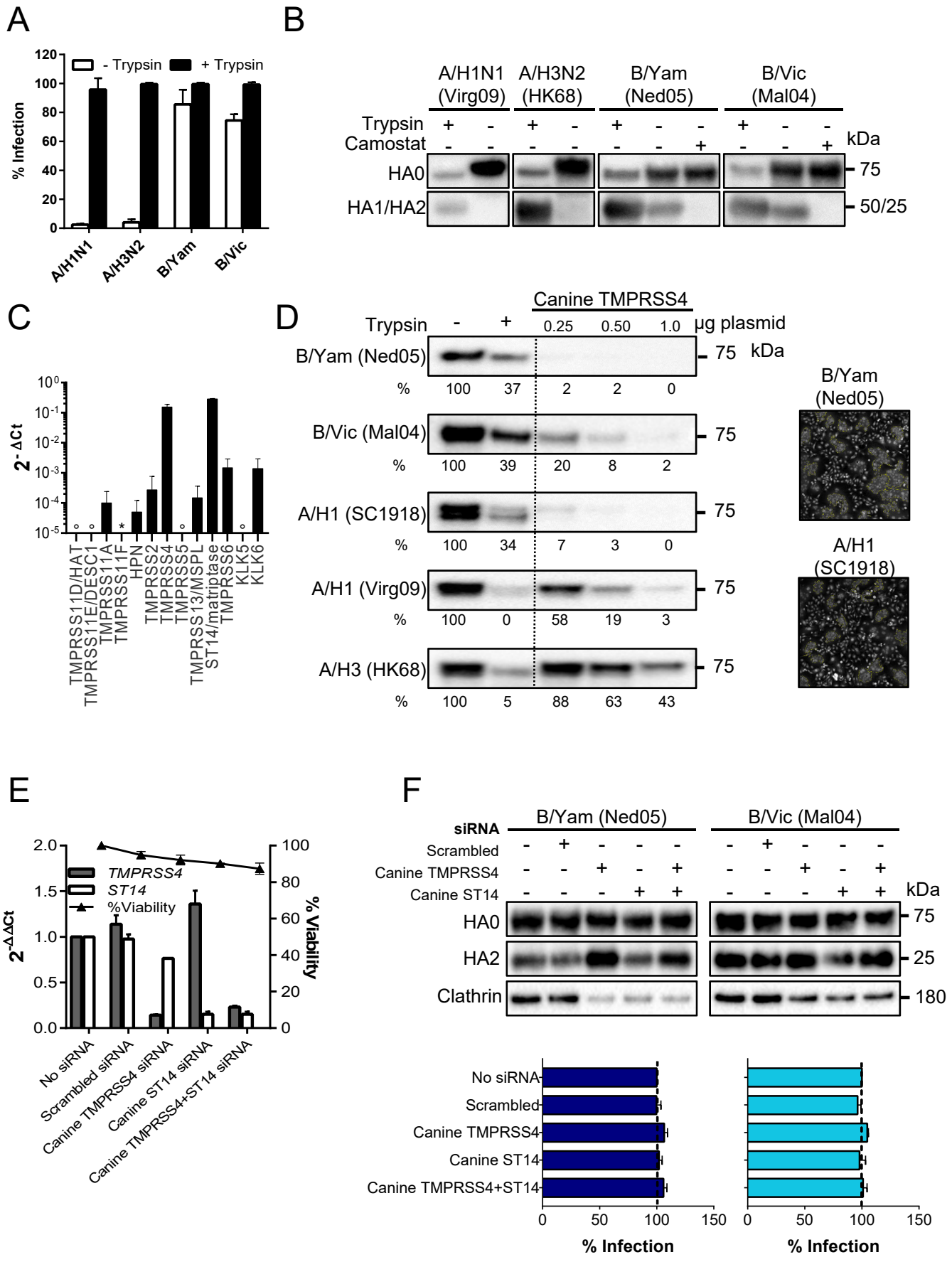
A
- Trypsin
+ Trypsin
% Infection
A/H1N1
A/H3N2
B/Yam
B/Vic
B
A/H1N1 (Virg09)
A/H3N2 (HK68)
B/Yam (Ned05)
B/Vic (Mal04)
Trypsin
Camostat
kDa
HA0
HA1/HA2
75
50/25
C
2-ΔCt
TMPRSS11D/HAT
TMPRSS11E/DESC1
TMPRSS11A
TMPRSS11F
HPN
TMPRSS2
TMPRSS4
TMPRSS5
TMPRSS13/MSPL
ST14/matriptase
TMPRSS6
KLK5
KLK6
D
Canine TMPRSS4
Trypsin
0.25
0.50
1.0
µg plasmid
B/Yam (Ned05)
B/Vic (Mal04)
A/H1 (SC1918)
A/H1 (Virg09)
A/H3 (HK68)
%
100 37 2 2 0
100 39 20 8 2
100 34 7 3 0
100 0 58 19 3
100 5 88 63 43
E
2-ΔΔCt
% Viability
TMPRSS4
ST14
%Viability
No siRNA
Scrambled siRNA
Canine TMPRSS4 siRNA
Canine ST14 siRNA
Canine TMPRSS4+ST14 siRNA
F
siRNA
B/Yam (Ned05)
B/Vic (Mal04)
Scrambled
Canine TMPRSS4
Canine ST14
HA0
HA2
Clathrin
No siRNA
Scrambled
Canine TMPRSS4
Canine ST14
Canine TMPRSS4+ST14
% Infection
% Infection

986 **Figure 6. MDCK cells contain high levels of HA-activating TMPRSS4.**

987 (A, B) IAV or IBV replication in MDCK cells in the presence or absence of trypsin. Panel
988 A: % infected cells at day 3 p.i., quantified by high-content imaging of NP. Mean ± SEM of
989 two experiments performed in quadruplo. Panel B: HA0 cleavage state at day 3 p.i. in cells
990 receiving 0 or 10 μM camostat. (C) Expression of TTSP and KLK proteases in MDCK cells
991 (normalized to canine *GAPDH* and *HMBS*). °Undetermined; *no data (no dog mRNA
992 sequence was available to design primers). (D) Canine TMPRSS4 activates the HAs of
993 IAV and IBV. Western blot, from left to right: HA0 band in HEK293T cells receiving no
994 protease, exogenous trypsin, or the canine TMPRSS4 plasmid at three different
995 concentrations. Under each lane, the HA0 band intensity is given (normalized to clathrin
996 and expressed relative to the no trypsin condition). Photographs: polykaryon formation in
997 HeLa cells undergoing co-expression of HA and canine TMPRSS4. (E, F) Effect of
998 TMPRSS4 and/or ST14/matriptase knockdown in MDCK cells. Panel E: mRNA levels at
999 24 h post siRNA transfection, normalized to canine *HMBS* and *GAPDH* and shown as the
1000 fold change *versus* untransfected control. Panel F: siRNA-transfected cells were infected
1001 with B/Yam or B/Vic virus, and at day 3 p.i., HA0 cleavage state was determined by
1002 western blot and virus infection was assessed by high-content imaging of NP.

Figure 7

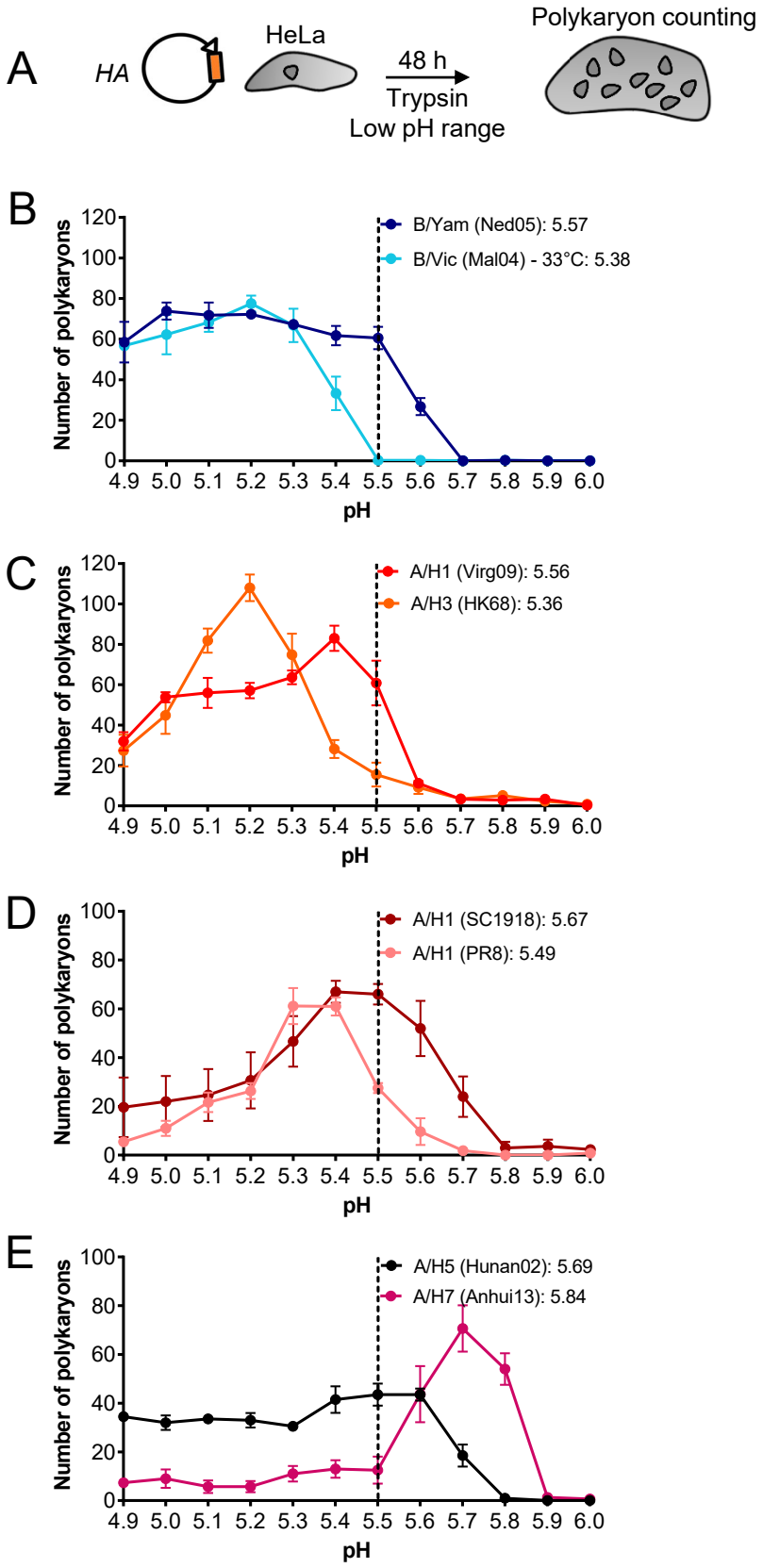
A
HA
HeLa
48 h
Trypsin
Low pH range
Polykaryon counting
B
B/Yam (Ned05): 5.57
B/Vic (Mal04) - 33°C: 5.38
Number of polykaryons
pH
C
A/H1 (Virg09): 5.56
A/H3 (HK68): 5.36
Number of polykaryons
pH
D
A/H1 (SC1918): 5.67
A/H1 (PR8): 5.49
Number of polykaryons
pH
E
A/H5 (Hunan02): 5.69
A/H7 (Anhui13): 5.84
Number of polykaryons
pH

1003 **Figure 7. IBV HA exhibits a similar fusion pH as human-adapted IAV HAs.**

1004 (A) Experiment set-up. HA-expressing HeLa cells were activated with exogenous trypsin,
1005 then exposed to a range of acidic buffers to induce cell-cell fusion. (B, C, D, E) Curves
1006 showing the number of polykaryons in function of the pH applied to trigger HA. Data are
1007 the mean ± SEM of two independent experiments, each performed in triplicate. The insets
1008 show the fusion pH values, defined as the pH at which the number of polykaryons was
1009 50% of the maximum number.

Figure 8

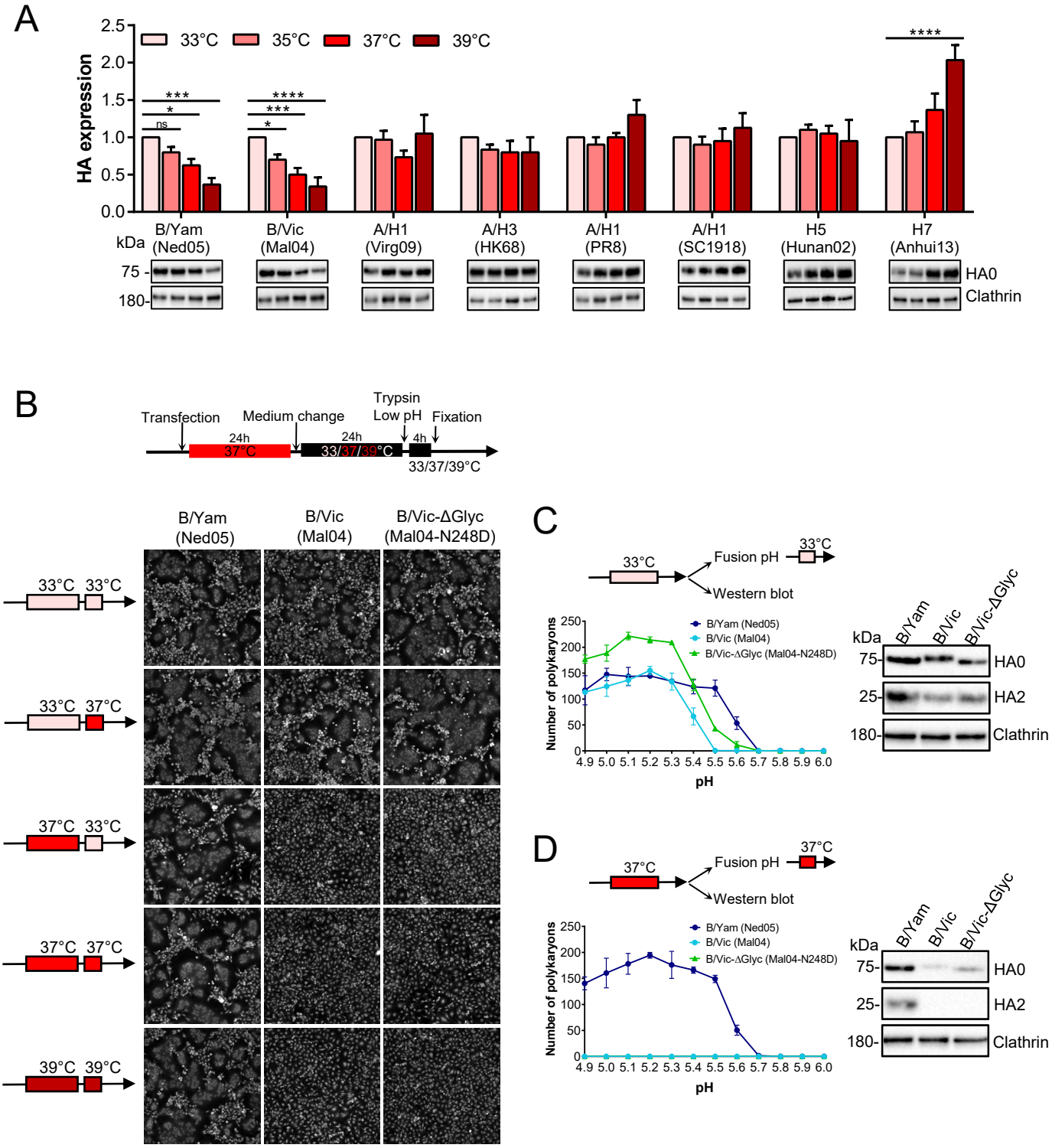
A
33°C
35°C
37°C
39°C
HA expression
2.5
2.0
1.5
1.0
0.5
0.0
***
*
ns
****
***
*
****
B/Yam (Ned05)
B/Vic (Mal04)
A/H1 (Virg09)
A/H3 (HK68)
A/H1 (PR8)
A/H1 (SC1918)
H5 (Hunan02)
H7 (Anhui13)
kDa
75 -
180-
HA0
Clathrin
B
Transfection
Medium change
Trypsin
Low pH
Fixation
24h
37°C
24h
33/37/39°C
4h
33/37/39°C
B/Yam (Ned05)
B/Vic (Mal04)
B/Vic-ΔGlyc (Mal04-N248D)
33°C 33°C
33°C 37°C
37°C 33°C
37°C 37°C
39°C 39°C
C
33°C
Fusion pH
33°C
Western blot
Number of polykaryons
B/Yam (Ned05)
B/Vic (Mal04)
B/Vic-ΔGlyc (Mal04-N248D)
pH
4.9 5.0 5.1 5.2 5.3 5.4 5.5 5.6 5.7 5.8 5.9 6.0
kDa
B/Yam
B/Vic
B/Vic-ΔGlyc
75-
25-
180-
HA0
HA2
Clathrin
D
37°C
Fusion pH
37°C
Western blot
Number of polykaryons
B/Yam (Ned05)
B/Vic (Mal04)
B/Vic-ΔGlyc (Mal04-N248D)
pH
4.9 5.0 5.1 5.2 5.3 5.4 5.5 5.6 5.7 5.8 5.9 6.0
kDa
B/Yam
B/Vic
B/Vic-ΔGlyc
75-
25-
180-
HA0
HA2
Clathrin

1010 **Figure 8. IBV HA prefers a temperature of 33°C for protein expression, explaining**
1011 **temperature-restricted fusion of B/Vic HA.**

1012 (A) HeLa cells were transfected with the indicated HA plasmids and incubated during 48
1013 h at four different temperatures. The graphs show quantitative western blot data for HA0
1014 band intensity, normalized to clathrin, and expressed relative to the HA0 band seen at
1015 33°C. Data are the mean ± SEM (N=3). *P*-values: *< 0.05, **< 0.01, ****≤ 0.0001 (ordinary
1016 one-way ANOVA, followed by Dunnett's test). (B, C, D) Polykaryon formation in IBV HA-
1017 transfected HeLa cells exposed to different temperatures during the stages of HA
1018 expression (starting 24 h post transfection) or cell-cell fusion. Panel B: fusion induced by
1019 a pH 5.0 buffer. Panel C and panel D: number of polykaryons in function of pH, after HA
1020 expression at 33°C (C) or 37°C (D). The western blots show the corresponding HA levels
1021 after trypsin activation.

Figure 9

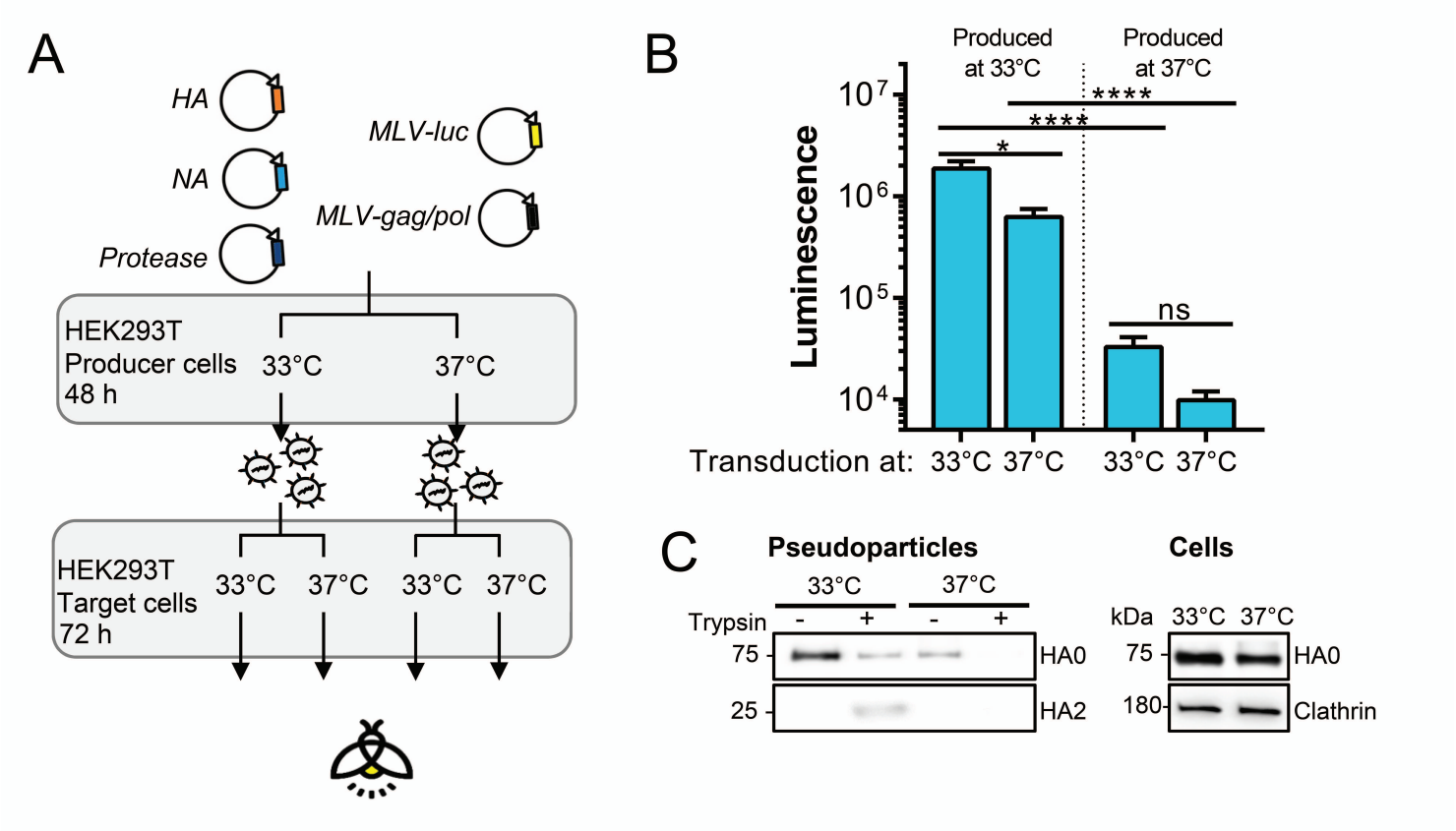

Figure 9. Pseudoparticles carrying B/Victoria HA require 33°C for infectivity. (A) Experiment set-up. Pseudoparticles carrying B/Vic (Mal04) HA and NA were produced at 33°C or 37°C, activated with trypsin, and transduced into HEK293T cells at 33°C or 37°C. (B) Infectivity of produced particles as measured by luminescence readout 3 days p.i. (C) HA levels in released pseudoparticles collected by ultracentrifugation and in HEK293T producer cells.